Accepted Manuscript

Discovery of 6-(difluoro(6-(4-fluorophenyl)-[1,2,4]triazolo[4,3-*b*][1,2,4]triazin-3-yl)methyl)quinoline as a highly potent and selective c-met inhibitor

Zhengsheng Zhan, Xia Peng, Qiufeng Liu, Fang Chen, Yinchun Ji, Shanyan Yao, Yong Xi, Yipeng Lin, Tiantian Chen, Yechun Xu, Jing Ai, Meiyu Geng, Wenhu Duan

PII: S0223-5234(16)30259-8

DOI: 10.1016/j.ejmech.2016.03.076

Reference: EJMECH 8501

To appear in: *European Journal of Medicinal Chemistry*

Received Date: 11 January 2016

Revised Date: 22 March 2016

Accepted Date: 25 March 2016

Please cite this article as: Z. Zhan, X. Peng, Q. Liu, F. Chen, Y. Ji, S. Yao, Y. Xi, Y. Lin, T. Chen, Y. Xu, J. Ai, M. Geng, W. Duan, Discovery of 6-(difluoro(6-(4-fluorophenyl)-[1,2,4]triazolo[4,3-*b*][1,2,4]triazin-3-yl)methyl)quinoline as a highly potent and selective c-met inhibitor, *European Journal of Medicinal Chemistry* (2016), doi: 10.1016/j.ejmech.2016.03.076.

Graphical Abstract

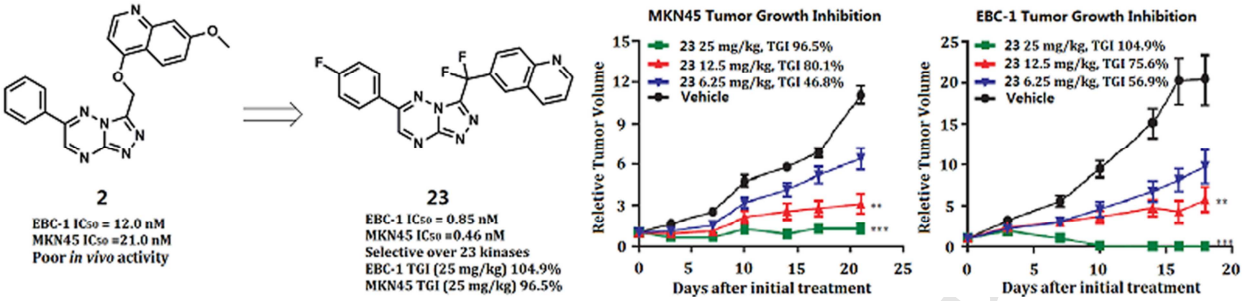

Discovery of 6-(Difluoro(6-(4-fluorophenyl)-[1,2,4]triazolo[4,3-*b*][1,2,4]triazin-3-yl)methyl)quinoline as a Highly Potent and Selective c-Met Inhibitor

Zhengsheng Zhan[a,§], Xia Peng[b,§], Qiufeng Liu[c,§], Fang Chen[a,§], Yinchun Ji[b], Shanyan Yao[a], Yong Xi[b], Yipeng Lin[a], Tiantian Chen[c], Yechun Xu[c,*], Jing Ai[b,*], Meiyu Geng[b,*], Wenhu Duan[a,*]

[a]Department of Medicinal Chemistry, Shanghai Institute of Materia Medica, Chinese Academy of Sciences (CAS), 555 Zu Chong Zhi Road, Shanghai 201203, China

[b]Division of Antitumor Pharmacology, State Key Laboratory of Drug Research, Shanghai Institute of Materia Medica, Chinese Academy of Sciences (CAS), 555 Zu Chong Zhi Road, Shanghai 201203, China

[c]CAS Key Laboratory of Receptor Research, Drug Discovery and Design Center, Shanghai Institute of Materia Medica, Chinese Academy of Sciences (CAS), 555 Zu Chong Zhi Road, Shanghai 201203, China

*(W.D.) E-mail: whduan@simm.ac.cn. Phone: +86-21-50806032.

*(M.G.) E-mail: mygeng@simm.ac.cn.

*(J.A.) E-mail: jai@simm.ac.cn.

*(Y.X.) E-mail: ycxu@simm.ac.cn.

[§](Z.Z., X.P., Q.L., and F.C.) These authors contributed equally to this work.

ABSTRACT

c-Met/HGF overexpression has been detected in many human malignancies including tumors which are resistant to anticancer therapy. Disrupting the aberrant c-Met/HGF axis has enjoyed significant progress in both preclinical and clinical antitumor campaign. To eliminate the OCH_2-related metabolic deficiency of our previously reported triazolotriazine **2**, we synthesized a series of CH_2-/CF_2-linked triazolotriazines and assessed their c-Met activities, leading to the highly potent compound **23** with IC_{50} values of 0.24 nM of enzymatic activity in c-Met and 0.85 nM of cellular activity in EBC-1 cancer cell line, as well as with complete tumor regression in EBC-1 xenograft mice model at dose of 25 mg/kg via oral administration. Based on its potent anti-proliferative activities and favorable pharmacokinetic properties, **23** has been selected as a drug candidate for preclinical investigation.

1. INTRODUCTION

The receptor tyrosine kinase c-Met, also known as hepatocyte growth factor receptor (HGFR), is a disulfide-linked transmembrane heterodimer composed of a short extracellular α chain and a membrane spanning β chain.[1, 2] Physiologically, HGF/c-Met axis mediates a diverse array of biological processes such as branching morphogenesis, migration, motility, proliferation, survival, wound healing, and angiogenesis, during embryonic development and tissue repair.[3-5] Aberrant c-Met signaling activation due to gene amplification, rearrangement, point mutation, as well as autocrine or paracrine HGF stimulation has been involved in the progression of many types of human malignancies.[6-12] Importantly, overexpression of HGF and/or c-Met has been associated with poor prognosis or metastatic progression. In addition, HGF/c-Met over-activation engaged in mediating intrinsic or acquired resistance to targeted therapies. For example, *MET* amplification correlates with approximately 20% of NSCLC patients developing acquired resistance against EGFR inhibitors.[13, 14] Thus, c-Met axis has emerged as a promising target for therapeutic medication of cancer.

Recently, HGF/c-Met biological antagonists, antibodies against c-Met or HGF, and small-molecule c-Met inhibitors have been employed as the strategies to inhibit the abnormal

c-Met/HGF axis for clinical anticancer campaign.[15-25] Small-molecule c-Met inhibitors can be roughly divided into ATP-competitive and non-ATP-competitive inhibitors.[26] Most of the c-Met inhibitors in clinical development are ATP-competitive. ATP-competitive c-Met inhibitors of the first generation usually target other kinases, for example, BMS-777607 is simultaneously active against c-Met and other receptor tyrosine kinases (AXL and Ron),[27] and XL184 inhibits VEGFR-2 besides c-Met.[28, 29] While the inhibitors of the second generation all share a relatively conserved structure which bind to the ATP binding pocket in a "U" shape, displaying high selectivity,[30, 31] representatively, JNJ38877605,[32] AMG337,[33] and INCB28060[34] are selective c-Met inhibitors (Figure 1). During the development of selective c-Met inhibitors, the OCH_2-linked molecule **1** (Figure 2) suffered O-dealkylation metabolism.[33] Similar problem emerged in our previously reported O-linked triazolotriazine **2**,[35] this compound possessed potent *in vitro* c-Met activity, but showed poor *in vivo* antitumor activities in the c-Met-driven xenograft models through oral administration (data not shown). The previous approach to eliminate such a liability was to replace the OCH_2 linker with $NHCH_2$ (**1a**) or $CHCH_3$ (**1b**), leading to a significant improvement in the metabolic properties (Figure 2).[33, 36] Here, we introduced a more robust carbon linkage, such as CH_2 or CF_2 to eliminate the metabolic deficiency (Figure 2), resulting in the identification of the highly potent and selective c-Met inhibitor 6-(difluoro(6-(4-fluorophenyl)-[1,2,4]triazolo[4,3-*b*][1,2,4]triazin-3-yl)methyl)quinoline as an antitumor agent for preclinical study.

<Figure 1>

<Figure 2>

2. RESULTS AND DISCUSSION

2.1. CH2- /CF2-Linked Triazolotriazines

To improve the metabolic liability of compound **2**, we designed and synthesized a series of CH_2-/CF_2-linked triazolotriazines. The enzymatic and cellular activities of the CH_2-linked triazolotriazines were summarized in Table 1. Compared with the lead compound **2**, compounds **3**−**21** exhibited decreased c-Met enzymatic potency. Among them, analogues **3**, **9**, **10**, and **14**

outperformed their counterparts with c-Met IC_{50} values ranging from 0.42 nM to 0.59 nM; the indole derivatives **19**, **20**, and **21** displayed a significant loss in both enzymatic and cellular activities, suggesting that the quinoline segment was essential to maintaining good c-Met potency.

Given that CH_2 linker might also suffer from metabolic instability[37], we further replaced the CH_2 linker with a CF_2 linker. To this end, the CF_2 linkage version of four CH_2-linked compounds (**3**, **12**, **14**, and **16**) with excellent enzymatic and cellular potency were prepared. As shown in Table 2, the CF_2-linked analogues **24**, **25**, and **27** maintained the enzymatic potency compared with their CH_2-linked analogues **12**, **14**, and **16**, respectively. The 6-phenyl CF_2-linked compound **22** displayed a six-fold drop in potency compared to its counterpart **3**; to our delight, when replacement of this phenyl with 4-fluorophenyl in the structure of **22**, the resulting analogue **23** displayed a nearly twelve-fold increase in enzymatic potency compared to **22** and was equipotent to the lead compound **2**. To explore the isosteric effect, furan analogue **26** was synthesized, and it was three-fold more potent than the thiophene analogue **24** in c-Met enzyme. Given these enzymatic data, the CF_2-linked analogues with excellent enzymatic activity (**23**, **25**, **26**, and **27**) were assayed in c-Met-addicted EBC-1 cell line, and they displayed sub-nanomolar to nanomolar IC_{50} values. Therefore, compounds **23**, **25**, **26**, and **27** were chosen for further evaluation.

<Table 1>

<Table 2>

2.2. Selection of Drug Candidate

The highly potent compounds **23**, **25**, **26**, and **27** were assessed for their pharmacokinetic (PK) profiles. As shown in Table 3, the PK data of **23**, **25**, **26**, and **27** were obtained in rats after single *iv* (2 mg/kg), and *po* (10 mg/kg) administration (*iv* dose of **25** was increased to 10 mg/kg). Different from their similarity of *in vitro* cellular activity, compound **25** showed low bioavailability (9.4%) and $AUC_{0-\infty}$. To identify the candidate for further profiling, compounds **23**, **26**, and **27** with both potent target inhibition and optimal PK properties were evaluated in the EBC-1 xenograft model. Mice bearing EBC-1 cancer cells were administrated the selected compounds orally twice daily for 21 days at the indicated doses. Body weight of the mice and

volume of the tumor were measured twice a week. As summarized in Table 4, **23** and **27** showed significant inhibition on tumor growth, and tumor regression was observed at the dose of 25 mg/kg, while **26** showed much weaker tumor growth inhibition (TGI = 65.8% @ 25 mg/kg). Of note, a body weight increase was observed at both doses of **23**-treated groups whereas weight loss emerged in **27**-treated (25 mg/kg) group, indicating low toxicity of compound **23** (data not shown). Based on the above results, compound **23** stood out as a new orally-available c-Met inhibitor with high *in vitro* and *in vivo* activities. Therefore, compound **23** was elected for further evaluation.

<Table 3>

<Table 4>

2.3. X-ray Co-Crystal Structure of Compound 23 with c-Met kinase domain

In order to elucidate the structure based activity of **23** to c-Met, we determined the co-crystal structure of the c-Met kinase domain in complex with **23**. In general, **23** bound into the ATP binding pocket of c-Met with a "U shape" and the kinase domain adopted a "DFG-in" inactive conformation (Figure 3). The detailed structure analysis revealed that the quinoline moiety of the compound occupied the adenosine binding site by forming a canonical hydrogen bond (H-bond) with the main-chain NH of Met1160 at the hinge region (Figure 3B). Replacement of the quinoline segment with an indole core would disrupt such a H-bonding interaction, which may explain the significant potency loss of **19**, **20**, **21** which all contain the indole core instead of the quinolone in **23** (Table 1). In addition, the triazolotriazine ring, the other essential part of **23**, formed the π-π stacking interactions with Tyr1230 at the activation loop and meanwhile a H-bond was formed between N1 of triazole and the main-chain NH of Asp1222 at the DFG motif. The substituted *p*-fluoryl phenyl group on the triazolotriazine core of **23** further stabilized the π-π stacking interactions (Figure 3B), contributing to the 10-fold biochemical potency increment against c-Met compared to **22** (Table 2). Therefore, the complex structure revealed the binding mode of **23** with the c-Met kinase domain and helped to explore the SARs of triazolotriazines as inhibitors of c-Met.

<Figure 3>

2.4. Compound 23 was a Potent and Highly Selective c-Met Inhibitor

Compound **23** was distinguished for its remarkable potency against c-Met kinase *in vitro* and *in vivo*. To determinate the kinases selectivity, we assayed its enzymatic activity in 23 additional kinases. As summarized in Table 5, compound **23** barely inhibited a panel of kinases, including c-Met family member Ron and highly homologous kinase Axl, Tyro3, c-Mer (IC_{50} >1 μM), indicating that **23** was a selective c-Met inhibitor.

<Table 5>

2.5. Compound 23 Inhibited c-Met Phosphorylation and Its Downstream Signaling Pathways

To further assess the kinase activity of **23** in cellular level, we measured its effect on the phosphorylation of c-Met and its downstream signaling molecules in the representative cancer cell or model cells (EBC-1, MKN45, BaF3/ TPR-Met, and U87MG cells) that cover the frequently occurring oncogenic forms of c-Met, including *MET* amplification, *MET* chromosomal rearrangement (*TPR-MET*), and HGF stimulation.[38, 39] Among these cells, EBC-1 and MKN45 cells harbor an amplified *MET* gene, and BaF3/TPR-Met cells stably express a constitutively active c-Met resulting from a chromosomal rearrangement, U87MG cells respond well to HGF stimulation. As shown in Figure 4, **23** significantly inhibited the phosphorylation of c-Met and its downstream signaling molecules (Akt and Erk)[38, 39] with a complete abolishment at 10 nM in each of these cell lines. These results suggested that **23** effectively suppressed c-Met activation and its signaling, regardless of the mechanistic complexity in c-Met activation across different cellular contexts.

<Figure 4>

2.6. Compound 23 Significantly Inhibited c-Met-addicted Proliferation of Human Cancer Cells

Activated c-Met is known to trigger cancer cell proliferation.[5] Therefore, we assessed the effect of **23** on cell proliferation in a broad panel of human cancer cell lines harboring different backgrounds of c-Met expression/activation. Compound **23** significantly inhibited the proliferation of the c-Met-constitutively activated EBC-1, and MKN-45 cells, with IC_{50} values of 0.85 nM and

0.46 nM, respectively (Table 6). Moreover, **23** effectively inhibited the proliferation of the genetically engineered BaF3/TPR-Met cells, which featured c-Met-dependent cell growth. In contrast, **23** showed over 10000-fold less potency in cells with low c-Met expression or activation (Figure 5). These data indicated that **23** specifically inhibited c-Met-dependent cancer cell proliferation.

<Figure 5>

<Table 6>

2.7. Compound 23 Inhibited c-Met-addicted Cell Migration, Invasion, and Scattering

In addition to the modulation of cell proliferation, activation of the HGF/c-Met axis promotes cell migration and invasion, which contributes to the metastatic characteristics of malignant cells.[40] Thus the impact of **23** in this regard was evaluated by Transwell-based migration and invasion assays of HGF-treated NCI-H441 cells. The results showed that **23** strongly suppressed HGF-induced cell migration and invasion in a dose-dependent manner (Figure 6A, B).

Activated HGF/c-Met signaling, also known to promote the cell scattering that stimulates cells to abandon their original environment, is a hallmark of cancer invasiveness and metastasis.[41] Since HGF stimulation could result in disruption and scattering of the MDCK cell colonies, we assayed the effect of **23** on cell scattering behavior using HGF-stimulated MDCK cells. As shown in Figure 6C, compound **23** inhibited the HGF-induced cell scattering of MDCK cells in a dose-dependent manner, completely blocking cell spreading at the dose of 10 nM.

Together, the above data suggested that **23** significantly impaired the cell motility and invasiveness mediated by the HGF/c-Met axis.

2.8. Compound 23 Suppressed c-Met-mediated Invasive Growth

c-Met activation in epithelial cells is known to induce a series of biological responses, including migration, matrix degradation, cell multiplication, and survival, which collectively gives rise to a unique multistep program known as invasive growth.[42] *In vitro*, this morphogenetic program was recapitulated by stimulating the suspended MDCK epithelial cells that cultured in a three-dimensional extracellular matrix (collagen) with HGF.[43, 44] We evaluated the inhibitory efficacy of **23** in this phenotype. As expected, MDCK cells in the absence of HGF displayed the round cysts, whereas HGF-stimulated MDCK cells formed the multicellular-branched structures. The branching morphogenesis of HGF-stimulated MDCK cells was obviously inhibited by compound **23** (Figure 6D), indicating that **23** suppressed the c-Met-mediated invasive growth phenotype.

<Figure 6>

2.9. In vivo c-Met-driven Tumor Growth Inhibition Studies of Compound 23

To further determinate the *in vivo* antitumor features of compound **23**, we assessed it in MKN45 and EBC-1 xenograft models. As shown in Figure 7, **23** displayed significant antitumor activity in a dose-dependent manner in both tumor xenografts. For the MKN45 model, treatment with **23** at 6.25, 12.5, and 25 mg/kg resulted in significant tumor growth inhibition, with an inhibitory rate of 46.8%, 80.1%, and 96.5%, respectively (Figure 7A). Similar results were observed in the EBC-1 xenograft (Figure 7B). Moreover, partial or complete tumor regression was observed in the EBC-1 model at the dose of 25 mg/kg. At all doses tested, **23** was well tolerated with no observatory weight loss (data not shown).

<Figure 7>

3. CHEMISTRY

The preparation of **3**−**27** is summarized in Scheme 1. Intermediates **52**−**68**, prepared according to the literature method,[35] were condensed with a carboxylic acid under the participation of the coupling reagents hydroxybenzotriazole (HOBT) and 1-ethyl-3-(3-dimethylaminopropyl) carbodiimide hydrochloride (EDCI) at ambient temperature to

give **28**−**51**. Intermediates **28**−**51** were cyclized to the triazolotriazines in acetic acid under reflux. However, only 5% yield of the desired product **23** was obtained in acetic acid under reflux, instead 85% yield of byproduct **23a** was formed. Therefore, the reaction condition should be optimized to improve the yield.

Scheme 2 summarizes the reaction conditions we investigated. We first employed pivalic acid in place of acetic acid in consideration that the steric effect of *tert*-butyl could inhibit the generation of the byproduct, but this reaction gave a low yield of **23** (32%) and a medium yield of byproduct **23b** (50%). Then using methanesulfonic acid as the cyclizing agent, **23** was obtained in 45% yield accompanying with 50% yield of intermediate **66** which was the decomposed product of **47**. When polyphosphoric acid (PPA) was used, the reaction improved slightly, and the yield of **23** increased to 55%, together with 40% yield of defluorinated byproduct **23c**.

Since the reaction generates one molecule of water during the formation of the triazolotriazine, we envisioned that the water generated *in situ* was the culprit of formation of **23c** which would be produced from **23** in presence of water, and such assumption was corroborated by preparing **23c** from **23** by adding small amount of water into PPA at the temperature of 140 ^{o}C (presented in Supporting Information). Thus 20% phosphorus pentoxide (w/w) was added to the reaction mixture to remove the generated water, and **23** was obtained in good yield (77%) accompanying with low yield of **23c** (20%).

High reaction temperature might also be the cause for defluorination of **23**, however when the reaction temperature was lowered from 140 ^{o}C to 90 ^{o}C, the reaction mixture became a gummy complex and could hardly be stirred. To decrease the high viscidity of the reaction mixture, DMF was added to the reaction mixture and the yield of **23** increased to 85%. To our delight, when the temperature further reduced to 65 ^{o}C, the yield of **23** increased to 90%, with only 1.5% yield of **23c**. Using the optimized condition, we prepared 10.5 kg of **23** for preclinical study.

<Scheme 1>

<Scheme 2>

4. CONCLUSION

A series of CH_2-/CF_2-linked triazolotriazines were designed and synthesized to overcome the metabolic deficiency of the OCH_2-linked triazolotriazine **2**. Among them, compounds **23**, **26**, and **27** possessed potent enzymatic and cellular c-Met activities and favorable PK profiles. Compound **23** outperformed its counterparts due to good anti-proliferative potency on EBC-1 xenograft model and low toxicity. Further evaluation unraveled that **23** specifically inhibited c-Met kinase activity, impairing c-Met phosphorylation and the downstream signaling across different oncogenic forms in c-Met overactivated cancer cells and model cells. Besides, **23**-treated inhibition was observed in c-Met driven cellular phenotype. Furthermore, **23** displayed significant antitumor activities in c-Met-driven EBC-1 and MKN45 xenografts. Given its excellent antitumor activities and favorable pharmacokinetic properties, **23** has been selected as an anticancer drug candidate for further development. We thereby optimized the process of preparation of **23** and prepared a sufficient amount of **23** for a preclinical study.

5. EXPERIMENTAL SECTION

5.1. General Methods for Chemistry

All reagents and solvents were purchased from commercial sources and used as received. ^{1}H NMR and ^{13}C NMR were generated in DMSO-d_6, $CDCl_3$, or CD_3OD on Varian Mercury 300, 400 or 500 NMR spectrometers. EI (Low-resolution and high-resolution mass spectra) were recorded on a Finnigan/MAT95 spectrometer. ESI (high-resolution mass spectra) were tested on a Waters Q-Tof Ultima apparatus. All melting points were determined on a Büchi B-510 melting point apparatus and are uncorrected. HPLC conditions were as follows: column, Agilent Eclipse Plus C18 3.5 μM, 4.6 mm×150 mm; solvent system, acetonitrile /water; flow rate 1.0 ml/min; UV detection, 254 nm; injection volume, 5 μL; temperature, 35 ℃. All the assayed compounds displayed a purity of >95% as confirmed by HPLC.

General Procedure for Preparation of Compounds 3−27

5.1.1. 6-((6-Phenyl-[1,2,4]triazolo[4,3-*b*][1,2,4]triazin-3-yl)methyl)quinoline (3) A mixture of 28 (500 mg, 1.403 mmol) and acetic acid (15 mL) was heated at 100 ^{o}C for 4 h. The reaction

mixture was then concentrated, and the residue was purified by silica gel chromatography, eluting with CH_2Cl_2/MeOH (20:1) to yield **3** as a white solid (385 mg, 81%), mp 224−226 °C. 1H NMR (300 MHz, DMSO-d_6) δ 9.31 (s, 1H), 8.87 (dd, J = 1.8, 5.2 Hz, 1H), 8.33 (dd, J = 1.2, 8.7 Hz, 1H), 8.16−8.19 (m, 2H), 7.98−8.01 (m, 2H), 7.85 (dd, J = 2.4, 8.7 Hz, 1H), 7.61−7.64 (m, 3H), 7.53 (q, J = 5.2, 8.7 Hz, 1H), 4.80 (s, 2H); 13C NMR (125 MHz, DMSO-d_6) δ 150.9, 148.3, 148.0, 147.9, 147.8, 147.3, 136.2, 134.4, 132.2, 132.1, 131.5, 129.8 (2C), 129.6, 128.3, 128.0 (3C), 122.2, 30.1. HRMS (ESI) calcd $[M + H]^+$ for $C_{20}H_{15}N_6$ 339.1353, found 339.1362.

5.1.2. 6-((6-(4-(Benzyloxy)phenyl)-[1,2,4]triazolo[4,3-*b*][1,2,4]triazin-3-yl)methyl)quinoline (4) The title compound was prepared from **29** using a method analogous to the synthesis of compound **3**. White solid (78%), mp 241−243 °C. ^{1}H NMR (300MHz, $CDCl_3$) δ 8.95 (s, 1H), 8.89 (d, J = 4.8 Hz, 1H), 8.11 (t, J = 7.8 Hz, 2H), 7.82−7.93 (m, 4H), 7.37−7.49 (m, 6H), 7.16 (d, J = 8.7 Hz, 2H), 5.18 (s, 2H), 4.80 (s, 2H); ^{13}C NMR (150 MHz, DMSO-d_6) δ 161.6, 150.9, 148.1, 147.9, 147.6, 147.5, 147.3, 137.0 (2C), 136.2, 134.5, 131.4, 129.7 (2C), 129.6, 129.0 (2C), 128.5, 128.3 (2C), 128.0, 124.5, 122.2, 116.1 (2C), 70.0, 30.1. HRMS (ESI) calcd $[M + H]^+$ for $C_{27}H_{21}N_6O$ 445.1771, found 445.1783.

5.1.3. 6-((6-(3,4-Dichlorophenyl)-[1,2,4]triazolo[4,3-*b*][1,2,4]triazin-3-yl)methyl)quinoline (5) The title compound was prepared from **30** using a method analogous to the synthesis of compound **3**. White solid (69%), mp >250 °C. ^{1}H NMR (300MHz, DMSO-d_6) δ 9.39 (s, 1H), 8.87 (dd, J = 1.8, 4.2 Hz, 1H), 8.41 (d, J = 2.1 Hz, 1H), 8.33 (d, J = 7.2 Hz, 1H), 8.18 (dd, J = 2.1, 8.4 Hz, 1H), 7.97−8.00 (m, 2H), 7.93 (d, J = 8.4 Hz, 1H), 7.83 (dd, J = 1.8, 8.7 Hz, 1H), 7.53 (dd, J = 2.1, 8.4 Hz, 1H), 4.81 (s, 2H); ^{13}C NMR (125 MHz, DMSO-d_6) δ 150.9, 148.0, 147.9, 147.8, 147.3, 146.2, 136.2, 134.9, 134.3, 132.8, 132.7, 132.0, 131.5, 129.9, 129.6, 128.3, 128.1, 128.0, 122.2, 30.1. HRMS (ESI) calcd $[M + Na]^+$ for $C_{20}H_{12}Cl_2N_6Na$ 429.0393, found 429.0399.

5.1.4. 6-((6-(3-Nitrophenyl)-[1,2,4]triazolo[4,3-*b*][1,2,4]triazin-3-yl)methyl)quinoline (6) The title compound was prepared from **31** using a method analogous to the synthesis of compound **3**. White solid (88%), mp 225−227 °C. ^{1}H NMR (300MHz, DMSO-d_6) δ 9.46 (s, 1H), 8.47−8.91 (m, 2H), 8.61 (d, J = 8.1 Hz, 1H), 8.48 (dd, J = 1.5, 4.8 Hz, 1H), 8.34 (d, J = 8.1 Hz, 1H), 7.81−8.01 (m, 4H), 7.53 (dd, J = 3.9, 8.4 Hz, 1H), 4.83 (s, 2H); ^{13}C NMR (150 MHz, DMSO-d_6) δ 151.0,

149.4, 148.3, 148.0, 147.9, 146.8, 147.5, 136.2, 134.7, 134.4, 133.3, 131.4, 129.6, 128.5, 128.2, 128.1, 127.6, 123.0, 122.1, 30.1. HRMS (EI) calcd M^+ for $C_{20}H_{13}N_7O_2$ 383.1131, found 383.1138.

5.1.5. 6-((6-(4-Chlorophenyl)-[1,2,4]triazolo[4,3-*b*][1,2,4]triazin-3-yl)methyl)quinoline (7) The title compound was prepared from **32** using a method analogous to the synthesis of compound **3**. White solid (79%), mp >250 °C. ^{1}H NMR (300MHz, $CDCl_3$) δ 8.94 (s, 1H), 8.88 (dd, J = 1.2, 3.9 Hz, 1H), 8.05−8.11 (m, 2H), 7.79−7.90 (m, 4H), 7.56 (d, J = 6.9 Hz, 2H), 7.41 (dd, J = 4.2, 8.4 Hz, 1H), 4.81 (s, 2H); ^{13}C NMR (150 MHz, DMSO-d_6) δ 150.9, 148.1, 147.9, 147.8, 147.3, 147.2, 137.1, 136.2, 134.4, 131.5, 131.1, 129.9 (2C), 129.8 (2C), 129.6, 128.3, 128.1, 122.2, 30.1. HRMS (ESI) calcd $[M + H]^+$ for $C_{20}H_{14}ClN_6$ 373.0963, found 373.0962.

5.1.6. 6-((6-(4-Bromophenyl)-[1,2,4]triazolo[4,3-*b*][1,2,4]triazin-3-yl)methyl)quinoline (8) The title compound was prepared from **33** using a method analogous to the synthesis of compound **3**. Yellow solid (79%), mp >250 °C. ^{1}H NMR (300MHz, DMSO-d_6) δ 9.37 (s, 1H), 8.87 (d, J = 3.9 Hz, 1H), 8.34 (d, J = 8.1 Hz, 1H), 8.14 (d, J = 7.2 Hz, 2H), 7.96−8.01 (m, 2H), 7.80−7.86 (m, 3H), 7.53 (q, J = 3.9, 7.2 Hz, 1H), 4.79 (s, 2H); ^{13}C NMR (125 MHz, DMSO-d_6) δ 150.9, 148.0, 147.9, 147.8, 147.3, 147.2, 136.2, 134.4, 132.8 (2C), 131.5, 131.4, 130.0 (2C), 129.6, 128.3, 128.0, 126.0, 122.2, 30.1. HRMS (ESI) calcd $[M + H]^+$ for $C_{20}H_{14}BrN_6$ 417.0458, found 417.0459.

5.1.7. 6-((6-(3-Methoxyphenyl)-[1,2,4]triazolo[4,3-*b*][1,2,4]triazin-3-yl)methyl)quinoline (9) The title compound was prepared from **34** using a method analogous to the synthesis of compound **3**. Pale yellow solid (82%), mp >250 °C. ^{1}H NMR (300MHz, DMSO-d_6) δ 9.23 (s, 1H), 8.47−8.91 (m, 2H), 8.67 (d, J = 8.1 Hz, 1H), 8.45 (dd, J = 1.5, 4.8 Hz, 1H), 8.31 (d, J = 8.1 Hz, 1H), 7.81−8.01 (m, 4H), 7.63 (dd, J = 3.9, 8.4 Hz, 1H), 4.83 (s, 2H), 3.88 (s, 3H); ^{13}C NMR (125 MHz, DMSO-d_6) δ 160.3, 150.9, 148.3, 148.0, 147.8 (2C), 147.3, 136.2, 134.4, 133.4, 131.4, 131.0, 129.6, 128.3, 128.0, 122.2, 120.4, 117.9, 113.1, 55.9, 30.2. HRMS (ESI) calcd $[M + H]^+$ for $C_{21}H_{17}N_6O$ 369.1458, found 369.1465.

5.1.8. 3-(3-(Quinolin-6-ylmethyl)-[1,2,4]triazolo[4,3-*b*][1,2,4]triazin-6-yl)phenol (10) The title compound was prepared from **35** using a method analogous to the synthesis of compound **3**. Yellow solid (63%), mp >250 °C. ^{1}H NMR (300MHz, DMSO-d_6) δ 10.55 (s, 1H), 9.24 (s, 1H), 8.47−8.91 (m, 2H), 8.56 (d, J = 8.1 Hz, 1H), 8.45 (dd, J = 1.5, 4.8 Hz, 1H), 8.21 (d, J = 8.1 Hz,

1H), 7.81−8.01 (m, 4H), 7.63 (dd, *J* = 3.9, 8.4 Hz, 1H), 4.79 (s, 2H); ^{13}C NMR (150 MHz, DMSO-d_6) δ 158.5, 150.9, 148.2, 148.0, 147.9, 147.7, 147.3, 136.2, 134.4, 133.3, 131.4, 130.9, 129.6, 128.3, 128.0, 122.1, 119.2, 119.0, 114.3, 30.1. HRMS (ESI) calcd $[M + H]^+$ for $C_{20}H_{15}N_6O$ 355.1302, found 355.1304.

5.1.9. 6-((6-(Quinolin-3-yl)-[1,2,4]triazolo[4,3-*b*][1,2,4]triazin-3-yl)methyl)quinoline (11) The title compound was prepared from **36** using a method analogous to the synthesis of compound **3**. White solid (82%), mp 219−221 °C. ^{1}H NMR (400MHz, DMSO-d_6) δ 9.54 (d, *J* = 2.1 Hz, 1H), 9.40 (s, 1H), 9.03 (d, *J* = 1.5 Hz, 1H), 8.83 (d, *J* = 4.2 Hz, 1H), 8.31 (d, *J* = 7.8 Hz, 1H), 8.21 (d, *J* = 8.1 Hz, 1H), 7.88−8.11 (m, 5H), 7.79 (t, *J* = 7.8 Hz, 1H), 7.53 (q, *J* = 4.8, 8.7 Hz, 1H), 4.92 (s, 2H); ^{13}C NMR (125 MHz, CF_3COOD) δ 154.2, 148.5, 148.4, 148.2, 147.5, 144.0, 143.7, 142.6, 139.2, 138.1, 137.0, 134.9, 132.4, 130.5, 129.8, 129.5, 128.8, 123.8, 122.0, 121.0, 120.3, 115.6, 29.1. HRMS (ESI) calcd $[M + H]^+$ for $C_{23}H_{16}N_7$ 390.1462, found 390.1463.

5.1.10. 6-((6-(Thiophen-2-yl)-[1,2,4]triazolo[4,3-*b*][1,2,4]triazin-3-yl)methyl)quinoline (12) The title compound was prepared from **37** using a method analogous to the synthesis of compound **3**. White solid (85%), mp 224−226 °C. ^{1}H NMR (300MHz, DMSO-d_6) δ 10.39 (s, 1H), 9.70 (br s, 1H), 9.00 (s, 1H), 8.87 (d, *J* = 4.2 Hz, 1H), 8.34 (d, *J* = 8.1 Hz, 1H), 7.91−7.99 (m, 2H), 7.65−7.79 (m, 3H), 7.54 (dd, *J* = 4.5, 8.4 Hz, 1H), 7.21 (dd, *J* = 0.9, 5.4 Hz, 1H); ^{13}C NMR (150 MHz, DMSO-d_6) δ 150.8, 148.4, 147.7, 147.5, 147.2, 136.2, 134.6, 134.5, 134.0, 132.1, 131.4, 129.5, 128.3, 128.0, 124.0, 122.1, 115.4, 30.1. HRMS (EI) calcd M^+ for $C_{18}H_{12}N_6S$ 344.0844, found 344.0853.

5.1.11.

6-((6-(1-Benzyl-1*H*-pyrazol-4-yl)-[1,2,4]triazolo[4,3-*b*][1,2,4]triazin-3-yl)methyl)quinoline (13) The title compound was prepared from **38** using a method analogous to the synthesis of compound **3**. White solid (83%), mp 237−239 °C. ^{1}H NMR (300MHz, $CDCl_3$) δ 8.87−8.85 (m, 1H), 8.68 (s, 1H), 8.11 (s, 1H), 8.07−8.02 (m, 3H), 7.81 (s, 1H), 7.78−7.74 (m, 1H), 7.40−7.28 (m, 6H), 5.40 (s, 2H), 4.73 (s, 2H); ^{13}C NMR (150 MHz, DMSO-d_6) δ 150.8, 148.3, 147.8, 147.4, 147.3, 143.8, 139.1, 137.2 (2C), 136.2, 134.4, 131.7, 131.5, 129.6, 129.1 (2C), 128.4, 128.2 (2C), 128.1, 122.1, 115.9, 55.8, 30.1. HRMS (ESI) calcd $[M + H]^+$ for $C_{24}H_{19}N_8$ 419.1727, found 419.1734.

5.1.12.

6-((6-(1-Methyl-1*H*-pyrazol-4-yl)-[1,2,4]triazolo[4,3-*b*][1,2,4]triazin-3-yl)methyl)quinoline (14) The title compound was prepared from **39** using a method analogous to the synthesis of compound **3**. White solid (81%), mp >250 °C. ^{1}H NMR (300MHz, DMSO-d_6) δ 9.11 (s, 1H), 8.85−8.86 (m, 1H), 8.65 (s, 1H), 8.35 (d, J = 6.9 Hz, 1H), 8.26 (s, 1H), 7.98−8.01 (m, 2H), 7.83 (d, J = 8.4 Hz, 1H), 7.49−7.53 (m, 1H), 4.71 (s, 2H), 3.96 (s, 3H); ^{13}C NMR (150 MHz, DMSO-d_6) δ 150.9, 148.3, 147.9, 147.4, 147.3, 143.9, 138.7, 136.2, 134.5, 132.1, 131.5, 129.6, 128.3, 128.1, 122.2, 115.5, 39.6, 30.1. HRMS (ESI) calcd $[M + H]^+$ for $C_{18}H_{15}N_8$ 343.1414, found 343.1417.

5.1.13.

6-((6-(1-Ethyl-1*H*-pyrazol-4-yl)-[1,2,4]triazolo[4,3-*b*][1,2,4]triazin-3-yl)methyl)quinoline (15) The title compound was prepared from **40** using a method analogous to the synthesis of compound **3**. White solid (88%), mp >250 °C. ^{1}H NMR (300MHz, $CDCl_3$) δ 8.88 (dd, J = 1.5, 4.5 Hz, 1H), 8.72 (s, 1H), 8.04−8.11 (m, 4H), 7.78−7.83 (m, 2H), 7.40 (q, J = 4.2, 8.1 Hz, 1H), 4.76 (s, 2H), 4.25−4.33 (m, 2H), 1.60 (t, J = 6.9 Hz, 3H); ^{13}C NMR (150 MHz, DMSO-d_6) δ 150.9, 148.3, 147.9, 147.4, 147.3, 143.9, 138.7, 136.2, 134.5, 131.8, 131.5, 129.6, 128.3, 128.1, 122.2, 115.3, 45.3, 30.1, 15.1. HRMS (EI) calcd M^+ for $C_{19}H_{16}N_8$ 356.1498, found 356.1501.

5.1.14.

6-((6-(1-Propyl-1*H*-pyrazol-4-yl)-[1,2,4]triazolo[4,3-*b*][1,2,4]triazin-3-yl)methyl)quinoline (16) The title compound was prepared from **41** using a method analogous to the synthesis of compound **3**. White solid (66%), mp 120−121 °C. ^{1}H NMR (300MHz, DMSO-d_6) δ 10.96 (br s, 1H), 9.08 (s, 1H), 8.69 (s, 1H), 8.28 (s, 1H), 7.67 (d, J = 7.5 Hz, 1H), 7.35 (t, J = 8.4 Hz, 2H), 6.99−7.09 (m, 2H), 4.57 (s, 2H), 4.18 (t, J = 6.9 Hz, 2H), 1.28−1.89 (m, 2H), 0.87 (t, J = 7.2 Hz, 3H); ^{13}C NMR (125 MHz, DMSO-d_6) δ 150.8, 148.3, 147.8, 147.4, 147.3, 143.9, 138.6, 136.2, 134.5, 131.5, 131.4, 129.6, 128.3, 128.1, 122.1, 115.2, 53.9, 30.1, 23.5, 11.3. HRMS (ESI) calcd $[M + H]^+$ for $C_{20}H_{19}N_8$ 371.1727, found 371.1734.

5.1.15. **Tert-butyl 4-(4-(3-(quinolin-6-ylmethyl)-[1,2,4]triazolo[4,3-*b*][1,2,4]triazin-6-yl)-1*H*-pyrazol-1-yl)piperidine-1-carboxylate (17)** The title compound was prepared from **42** using a method analogous to

the synthesis of compound **3**. White solid (14%), mp 112−114 °C. ^{1}H NMR (300MHz, $CDCl_3$) δ 8.89 (d, J = 3.9 Hz, 1H), 8.72 (s, 1H), 8.05−8.12 (m, 4H), 7.79−7.83 (m, 2H), 7.42 (q, J = 3.9, 7.8 Hz, 1H), 4.77 (s, 2H), 4.32−4.37 (m, 3H), 2.89−2.97 (m, 2H), 2.12−2.21 (m, 2H), 1.94−2.04 (m, 2H), 1.49 (s, 9H); ^{13}C NMR (150 MHz, DMSO-d_6) δ 154.3, 150.9, 148.4, 147.8, 147.4, 147.3, 143.9, 138.4, 136.2, 134.5, 131.5, 129.8, 129.6, 128.3, 128.1, 122.1, 115.3, 79.4, 59.2, 32.3 (2C), 30.1 (3C), 28.6 (3C). HRMS (ESI) calcd $[M + H]^+$ for $C_{27}H_{30}N_9O_2$ 512.2517, found 512.2531.

5.1.16.

6-((6-(1-(Piperidin-4-yl)-1*H*-pyrazol-4-yl)-[1,2,4]triazolo[4,3-*b*][1,2,4]triazin-3-yl)methyl)quinoline (18) A mixture of **17** (350 mg, 0.648 mmol), CF_3COOH (0.5 mL, 6.842 mmol), and DCM (25 mL) was stirred at room temperature for 5 h. The reaction mixture was then concentrated, and the residue was purified by silica gel chromatography, eluting with CH_2Cl_2/MeOH (10:1) to yield **18** as a white solid (59 mg, 21%), mp 125−127 °C. ^{1}H NMR (300 MHz, $CDCl_3$) δ 9.12 (s, 1H), 8.85−8.86 (m, 1H), 8.78 (s, 1H), 8.32−8.35 (m, 1H), 8.28 (s, 1H), 7.97−7.99 (m, 2H), 7.79−7.83 (m, 1H), 7.53 (q, J = 3.9, 7.8 Hz, 1H), 4.71 (s, 2H), 4.45−4.58 (m, 2H), 3.92−3.97 (m, 1H), 3.12−3.31 (m, 3H), 2.70−2.75 (m, 1H), 2.05−2.14 (m, 1H), 1.75−1.94 (m, 2H); ^{13}C NMR (150 MHz, DMSO-d_6) δ 150.9, 148.4, 147.8, 147.4, 147.3, 143.9, 138.4, 136.2, 134.5, 131.5, 129.8, 129.6, 128.3, 128.1, 122.1, 115.3, 59.2, 44.9 (2C), 32.9, 32.1, 30.1. HRMS (ESI) calcd $[M + H]^+$ for $C_{22}H_{22}N_9$ 412.1993, found 412.2002.

5.1.17. 3-((1*H*-indol-3-yl)methyl)-6-(4-(benzyloxy)phenyl)-[1,2,4]triazolo[4,3-*b*][1,2,4]triazine (19) The title compound was prepared from **43** using a method analogous to the synthesis of compound **3**. White solid (69%), mp 241−243 °C. ^{1}H NMR (300MHz, DMSO-d_6) δ 10.95 (br s, 1H), 9.29 (s, 1H), 8.15 (d, J = 9.0 Hz, 2H), 7.66 (d, J = 8.1 Hz, 1H), 7.32−7.50 (m, 7H), 7.24 (d, J = 9.0 Hz, 2H), 6.96−7.09 (m, 2H), 5.25 (s, 2H), 4.62 (s, 2H); ^{13}C NMR (150 MHz, DMSO-d_6) δ 161.5, 148.3, 147.7, 147.6, 147.3, 137.0, 136.6, 129.7 (2C), 129.0 (2C), 128.5, 128.3 (2C), 127.4, 124.6, 121.6, 119.1, 119.0, 116.1 (2C), 111.9, 108.4 (2C), 70.0, 20.7. HRMS (ESI) calcd $[M + H]^+$ for $C_{26}H_{21}N_6O$ 433.1771, found 433.1773.

5.1.18. 3-((1*H*-indol-3-yl)methyl)-6-(4-bromophenyl)-[1,2,4]triazolo[4,3-*b*][1,2,4]triazine (20) The title compound was prepared from **44** using a method analogous to the synthesis of compound

3. White solid (49%), mp 241−243 °C. ^{1}H NMR (300MHz, DMSO-d_6) δ 10.96 (br s, 1H), 9.32 (s, 1H), 8.14 (d, J = 8.4 Hz, 2H), 7.86 (d, J = 8.4 Hz, 2H), 7.68 (d, J = 7.8 Hz, 1H), 7.32−7.34 (m, 2H), 6.97−7.10 (m, 2H), 4.64 (s, 2H); ^{13}C NMR (125 MHz, DMSO-d_6) δ 148.5, 147.7, 147.6, 147.0, 136.6, 132.8 (2C), 131.5, 130.0 (2C), 127.3, 125.9, 124.6, 121.6, 119.0 (2C), 111.9, 108.3, 20.7. HRMS (ESI) calcd $[M + H]^+$ for $C_{19}H_{14}BrN_6$ 405.0458, found 405.0463.

5.1.19. 3-(3-((1*H*-indol-3-yl)methyl)-[1,2,4]triazolo[4,3-*b*][1,2,4]triazin-6-yl)phenol (21) The title compound was prepared from **45** using a method analogous to the synthesis of compound **3**. White solid (56%), mp 214−216 °C. ^{1}H NMR (300MHz, DMSO-d_6) δ 10.95 (br s, 1H), 9.92 (s, 1H), 9.26 (s, 1H), 7.57−7.69 (m, 3H), 7.44 (t, J = 7.8 Hz, 1H), 7.33−7.35 (m, 2H), 6.96−7.09 (m, 3H), 4.63 (s, 2H); ^{13}C NMR (150 MHz, DMSO-d_6) δ 158.5, 148.3, 147.9, 147.8, 147.7, 136.6, 133.4, 130.9, 127.3, 124.5, 121.7, 119.2, 119.1, 119.0 (2C), 114.2, 111.9, 108.4, 20.7. HRMS (ESI) calcd $[M + H]^+$ for $C_{19}H_{15}N_6O$ 343.1302, found 343.1303.

5.1.20. 6-(Difluoro(6-phenyl-[1,2,4]triazolo[4,3-*b*][1,2,4]triazin-3-yl)methyl)quinoline (22) The title compound was prepared from **46** using a method analogous to the synthesis of compound **3**. White solid (39%), mp 164−166 °C. ^{1}H NMR (300MHz, $CDCl_3$) δ 9.14 (s, 1H), 9.03 (d, J = 2.4 Hz, 1H), 8.25−8.33 (m, 3H), 8.00−8.10 (m, 3H), 7.60−7.67 (m, 3H), 7.54 (dd, J = 3.9, 8.7 Hz, 1H); ^{13}C NMR (150 MHz, DMSO-d_6) δ 153.1, 150.2, 149.3, 149.0, 148.8, 143.0 (t, J = 36.3 Hz), 137.6, 132.4, 131.6, 131.5 (t, J = 24.9 Hz), 130.4, 129.9 (2C), 128.1 (2C), 127.6, 127.4 (t, J = 5.6 Hz), 126.7, 123.0, 117.7 (t, J = 239.4 Hz). HRMS (ESI) calcd $[M + H]^+$ for $C_{20}H_{13}F_2N_6$ 375.1164, found 375.1168.

5.1.21.

6-(Difluoro(6-(4-fluorophenyl)-[1,2,4]triazolo[4,3-*b*][1,2,4]triazin-3-yl)methyl)quinoline (23) Method A: the title compound was prepared from **47** using a method analogous to the synthesis of compound **3**. Off-white solid (5%), mp 208−210 °C. ^{1}H NMR (300MHz, DMSO-d_6) δ 9.53 (s, 1H), 9.06 (dd, J = 1.8, 3.9 Hz, 1H), 8.61 (d, J = 8.4 Hz, 1H), 8.50 (s, 1H), 8.15−8.24 (m, 3H), 8.06 (dd, J = 1.8, 8.1 Hz, 1H), 7.69 (q, J = 3.9, 8.1 Hz, 1H), 7.51 (t, J = 9.0 Hz, 2H); ^{13}C NMR (100 MHz, DMSO-d_6) δ 166.0, 163.5, 152.9, 150.1, 149.1 (d, J = 86.8 Hz), 148.5, 143.1 (t, J = 35.6

Hz), 137.7, 131.6 (t, *J* = 24.9 Hz), 130.8 (d, *J* = 12.0 Hz, 2C), 130.1, 128.1 (d, *J* = 2.8 Hz), 127.5, 127.3 (t, *J* = 5.2 Hz), 127.2 (t, *J* = 5.1 Hz), 123.0, 118.4 (t, *J* = 239.5 Hz), 117.1 (d, *J* = 22.6 Hz, 2C). HRMS (ESI) calcd $[M + H]^+$ for $C_{20}H_{12}F_3N_6$ 393.1070, found 393.1074.

Method B: a mixture of 200 g polyphosphoric acid, 40 g phosphorus pentoxide, and 200 mL DMF was mechanically stirred, when the temperature reduced to about 45 ^oC, **47** (20 g, 0.0487 mol) was added to the mixture with stirring, the resulting complex was heated at 65 ^oC for 72 h. The gummy reaction complex was poured into ice with stirring until homogeneous phase formed, then ammonia water was added dropwise to alkalize the mixture, the brown solid was harvested by filtration. Then the brown solid was stirred in isopropanol for 3 h, after filtration and dry, yielded **23** as off-white solid (17.1 g, 90%).

5.1.22. 6-(Difluoro(6-(thiophen-2-yl)-[1,2,4]triazolo[4,3-*b*][1,2,4]triazin-3-yl)methyl)quinoline (24) The title compound was prepared from **48** using a method analogous to the synthesis of compound **3**. Pale yellow solid (41%), mp 227−229 °C. ^{1}H NMR (300MHz, $CDCl_3$) δ 8.99−9.01 (m, 2H), 8.23−8.33 (m, 3H), 8.10 (d, *J* = 8.7 Hz, 1H), 7.88 (d, *J* = 3.9 Hz, 1H), 7.72 (d, *J* = 5.4 Hz, 1H), 7.52 (q, *J* = 4.8, 8.7 Hz, 1H), 7.24−7.27 (m, 1H); ^{13}C NMR (150 MHz, DMSO-d_6) δ 153.1, 149.4, 149.0, 148.5, 146.3, 143.0 (t, *J* = 36.0 Hz), 137.8, 134.5, 134.0, 132.1, 131.5 (t, *J* = 24.6 Hz), 130.1, 127.7, 127.2 (t, *J* = 5.6 Hz), 126.7, 124.3, 123.1, 117.6 (t, *J* = 240.0 Hz). HRMS (EI) calcd M^+ for $C_{18}H_{10}F_2N_6S$ 380.0656, found 380.0660.

5.1.23. 6-(Difluoro(6-(1-methyl-1*H*-pyrazol-4-yl)-[1,2,4]triazolo[4,3-*b*][1,2,4]triazin-3-yl)methyl)quinoline (25) The title compound was prepared from **49** using a method analogous to the synthesis of compound **3**. White solid (43%), mp 238−240 °C. ^{1}H NMR (300MHz, $CDCl_3$) δ 9.02 (d, *J* = 1.8 Hz, 1H), 8.83 (s, 1H), 8.23−8.26 (m, 3H), 8.02−8.06 (m, 3H), 7.45−7.52 (m, 1H), 4.04 (s, 3H); ^{13}C NMR (125 MHz, DMSO-d_6) δ 153.0, 150.3, 149.1, 148.8, 145.0, 142.8 (t, *J* = 35.8 Hz), 138.9, 137.5, 132.4, 131.7 (t, *J* = 25.3 Hz), 130.3, 127.6, 127.3 (t, *J* = 6.3 Hz), 126.7, 123.0, 118.0 (t, *J* = 241.6 Hz), 115.1, 39.6. HRMS (ESI) calcd $[M + H]^+$ for $C_{18}H_{13}F_2N_8$ 379.1226, found 379.1230.

5.1.24. 6-(Difluoro(6-(furan-2-yl)-[1,2,4]triazolo[4,3-*b*][1,2,4]triazin-3-yl)methyl)quinoline (26) The title compound was prepared from **50** using a method analogous to the synthesis of

compound **3**. Yellow solid (39%), mp 217−219 °C. ^{1}H NMR (300MHz, $CDCl_3$) δ 9.08 (s, 1H), 9.02 (d, J = 3.9 Hz, 1H), 8.24−8.29 (m, 3H), 8.08 (d, J = 9.3 Hz, 1H), 7.78 (s, 1H), 7.48−7.52 (m, 1H), 7.39 (d, J = 3.3 Hz, 1H), 6.72 (d, J = 2.1 Hz, 1H); ^{13}C NMR (150 MHz, DMSO-d_6) δ 153.0, 149.5, 149.0, 148.7, 148.6, 146.5, 143.1 (t, J = 36.0 Hz), 141.4, 137.8, 131.6 (t, J = 24.8 Hz), 130.1, 127.6, 127.3 (t, J = 5.4 Hz), 126.8, 123.0, 118.0, 117.8 (t, J = 240.0 Hz), 113.8. HRMS (ESI) calcd $[M + H]^+$ for $C_{18}H_{11}F_2N_6O$ 365.0957, found 365.0961.

5.1.25.

6-(Difluoro(6-(1-propyl-1*H*-pyrazol-4-yl)-[1,2,4]triazolo[4,3-*b*][1,2,4]triazin-3-yl)methyl)quinoline (27) The title compound was prepared from **51** using a method analogous to the synthesis of compound **3**. Yellow solid (45%), mp 81−83 °C. ^{1}H NMR (300MHz, $CDCl_3$) δ 9.05 (s, 1H), 8.84 (s, 1H), 8.26 (m, 3H), 8.01−8.11 (m, 3H), 7.51 (m, 1H), 4.21 (t, J = 6.9 Hz, 2H), 1.90−2.00 (m, 2H), 0.98 (t, J = 7.5 Hz, 3H); ^{13}C NMR (125 MHz, DMSO-d_6) δ 153.0, 150.5, 149.2, 148.7, 145.1, 142.9 (t, J = 36.0 Hz), 138.9, 137.7, 133.0, 131.9 (t, J = 25.3 Hz), 130.3, 127.8, 127.3 (t, J = 6.4 Hz), 126.1, 123.4, 118.1 (t, J = 240.3 Hz), 115.7, 53.9, 23.4, 11.3. HRMS (ESI) calcd $[M + H]^+$ for $C_{20}H_{17}F_2N_8$ 407.1539, found 407.1545.

5.2. ELISA Kinase Assay

The effects of compounds on the activities of various tyrosine kinases were determined using enzyme-linked immunosorbent assays (ELISAs) with purified recombinant proteins. Briefly, 20 μg/mL poly $(Glu,Tyr)_{4:1}$ (Sigma, St Louis, MO, USA) was pre-coated in 96-well plates as a substrate. A 50-μL aliquot of 10 μmol/L ATP solution diluted in kinase reaction buffer (50 mmol/L HEPES [pH 7.4], 50 mmol/L $MgCl_2$, 0.5 mmol/L $MnCl_2$, 0.2 mmol/L Na_3VO_4, and 1 mmol/L DTT) was added to each well; 1 μL of various concentrations of compounds diluted in 1% DMSO (*v/v*) (Sigma, St Louis, MO, USA) were then added to each reaction well. DMSO (1%, *v/v*) was used as the negative control. The kinase reaction was initiated by the addition of purified tyrosine kinase proteins diluted in 49 μL of kinase reaction buffer. After incubation for 60 min at 37 °C, the plate was washed three times with phosphate-buffered saline (PBS) containing 0.1% Tween 20 (T-PBS). Anti-phosphotyrosine (PY99) antibody (100 μL; 1:500, diluted in 5 mg/mL BSA T-PBS) was then added. After a 30-min incubation at 37 °C, the plate was washed three times, and 100 μL

horseradish peroxidase-conjugated goat anti-mouse IgG (1:2000, diluted in 5 mg/mL BSA T-PBS) was added. The plate was then incubated at 37 °C for 30 min and washed 3 times. A 100-μL aliquot of a solution containing 0.03% H_2O_2 and 2 mg/mL *o*-phenylenediamine in 0.1 mol/L citrate buffer (pH 5.5) was added. The reaction was terminated by the addition of 50 μL of 2 mol/L H_2SO_4 as the color changed, and the plate was analyzed using a multi-well spectrophotometer (SpectraMAX 190, from Molecular Devices, Palo Alto, CA, USA) at 490 nm. The inhibition rate (%) was calculated using the following equation: $[1 - (A_{490}/A_{490\ control})] \times 100\%$. The IC_{50} values were calculated from the inhibition curves in two separate experiments.

5.3. Cell Culture

The human gastric cancer cell lines SNU-1, SNU-5,SNU-16, AGS, MGC-803, BGC-823, and BGC-7901; the human lung cancer cell lines SPC-A1, SPC-A4, Calu-3, NCI-H441, NCI-H661, NCI-H226, NCI-H3122, NCI-H596, and NCI-H1299; the human breast cancer cell line MDA-MB-231; the human colon cancer cell line HCT-116; the human renal cell adenocarcinoma cell line 786-O; the human epithelioid carcinoma cell line PANC-1 and the Madin-Daby canine kidney (MDCK) cell line were purchased from American Type Culture Collection (ATCC, Manassas, VA, USA). The hepatic carcinoma cell line SMMC-7721 and the human lung cancer cell lines HCC827,BEL-7404, NCI-H292, NCI-H358, NCI-H460 were obtained from the Institute of Biochemistry and Cell Biology, Chinese Academy of Sciences (Shanghai, China). The human gastric cell line MKN-45 and the human NSCLC cell line EBC-1 were purchased from Joint Conference of Restoration Branches (JCRB). The murine pre-B cell line BaF3 was obtained from ATCC and grown in RPMI 1640 containing 10% fetal bovine serum (FBS) and 10% WEHI-conditioned medium as a source of murine interleukin 3. The genetical architectures was generated from transfecting the BaF3 cell line with expression vector containing the *TPR-MET* cDNA (Addgene) and subsequent selecting in puromycin (Invitrogen Corporation). All the cell lines were routinely maintained in media according to the suppliers' recommendations. Except of special instructions, cell culture reagents were obtained from Life Technologies, Inc. Cells were routinely maintained according to recommendations of their suppliers.

5.4. Western Blot Analysis

U87MG cells were serum-starved for 24 h, treated with the indicated dose of **23** for 1 h at 37 °C, stimulated with HGF (100 ng/mL, PeproTech, Rocky Hill, NJ, USA) for 15 min, and then lysed in 1×sodium dodecyl sulfate (SDS) sample buffer. EBC-1, MKN-45, and BaF3/TPR-Met cells were treated with the indicated dose of **23** for 1 h at 37 °C and then lysed in 1×SDS sample buffer. The cell lysates were subsequently resolved by 10% SDS-PAGE and transferred to nitrocellulose membranes. The membranes were probed with the appropriate primary antibodies [c-Met (Santa Cruz, CA, USA), phospho-c-Met, phospho-ERK1/2, phospho-AKT, and AKT (all from Cell Signaling Technology, Beverly, MA, USA), and GAPDH (KangChen Biotech, Shanghai, China)] and then with horseradish peroxidase-conjugated anti-rabbit or anti-mouse IgG. The immunoreactive proteins were detected using an enhanced chemiluminescence detection reagent (Thermo Fisher Scientific, Rockford, IL, USA).

5.5. Cell Proliferation Assay

Cells were seeded in 96-well tissue culture plates. On the next day, the cells were exposed to various concentrations of compounds and further cultured for 72 h. Cell proliferation was then determined using sulforhodamine B (SRB, from Sigma-Aldrich, St Louis, MO, USA) or the thiazolyl blue tetrazolium bromide (MTT, from Sigma-Aldrich, St Louis, MO, USA) assay. The IC_{50} values were calculated by concentration-response curve fitting using the four-parameter method. Each reagent and concentration was tested at least in triplicate during each experiment, and each experiment was performed at least 2 times.

5.6. Cell Migration and Matrigel Invasion Assays

For the migration assays, 1.5×10^5 cells in serum-free media were placed into the upper chamber of an insert (8 μm pore size; Corning Inc.). For the invasion assays, 1.5×10^5 cells in serum-free media were placed into the upper chamber of an insert coated with Matrigel (BD Bioscience). Serum-free medium was added to the lower chamber with or without recombinant human HGF (100 ng/mL). After 24 h of incubation at 37 ^{o}C , the cells remaining on the upper

membrane were removed with cotton wool, whereas the cells that had migrated or invaded through the porous membrane were stained with 0.1% crystal violet for 15 min at room temperature. Finally, migrated and invasive cells were imaged in 5 different fields of each filter. Images were obtained using an Olympus BX51 microscope.

5.7. Cell-scatter Assay

MDCK cells (1.5×10^3 cells per well) were plated in 96-well plates and grown overnight. Increasing concentrations of **23** and HGF (100 ng/mL) were added to the appropriate wells, and the plates were incubated at 37 °C and 5% CO_2 for 24 h. The cells were fixed with 4% paraformaldehyde for 15 min at room temperature and then stained with 0.2% crystal violet, washed with water, and dried. Images were obtained using an Olympus IX51 microscope.

5.8. Cell Branching Morphogenesis Assay

MDCK cells at a density of 2×10^4 cells/mL in DMEM medium were mixed with an equal volume of collagen I solution and plated at 0.1 mL/well in a 96-well culture plate. After incubation for 60 min at 37 °C and 5% CO_2 to allow the collagen to gel, HGF (100 ng/mL) with or without **23** at various concentrations dissolved in 100 μL of growth medium was added to each well. The medium was replaced with fresh growth medium every 2 d. Images were obtained using an Olympus IX51 microscope after 5d.

5.9. S.c. Xenograft Models in Athymic Mice and in vivo Antitumor Activity Studies

Nude mice were used for all *in vivo* studies. The mice were housed and maintained under specific-pathogen free conditions in accordance with Institutional Animal Care and Use Committee. Cells at density of $5-10\times10^6$ in 200 μL firstly implanted s.c. into the right flank of each nude mice and then allowing to grow to 700−800 mm^3, defined as a well-developed tumor. After that, the well-developed tumors were cut into 1.5 mm^3 fragments and transplanted s.c. into the right flank of nude mice. When the tumor volume reached 100 to 200 mm^3, the mice were randomly assigned into vehicle and treatment groups (n = 6 in treated group, n = 12 in vehicle group). Vehicle groups were given vehicle alone, and treatment groups received **23** as indicated doses via *po* administration once daily for indicated days. The sizes of the tumors were measured

twice per week using microcaliper. The tumor volume (TV) was calculated as: TV = (length×width^2)/2 and the individual relative tumour volume (RTV) was calculated as follows: RTV = V_t/V_0, where V_t is the volume on each day, and V_0 is the volume at the beginning of the treatment. RTV was shown on indicated days as the median RTV ± SE indicated for groups of mice. Percent (%) inhibition values (TGI) were measured on the final day of study for drug-treated compared with vehicle-treated mice and are calculated as $100 \times \{1 - [(V_{\text{Treated Final day}} - V_{\text{Treated Day 0}}) / (V_{\text{Vehicle Final day}} - V_{\text{Vehicle Day 0}})]\}$. Significant differences between the treated versus the vehicle groups ($P \leq 0.05$) were determined using Student's t test.

5.10. Co-crystallization of 23 and c-Met

Co-crystallization of the c-Met kinase domain with the compound **23** was carried out by mixing a solution of the protein-ligand complex with an equal volume of precipitant solution (100 mM Tris-HCl pH 7.3, 5% isopropanol, 12% MPD, 12−14% PEG5KMME). The protein-ligand complex was prepared by adding the compound to the protein solution to a final concentration of 1 mM **23**. Co-crystallization utilized the vapour-diffusion method in hanging drops. Crystals were flash frozen in liquid nitrogen in the presence of well solution supplemented with 25% glycerol. Details of the crystal structure can be obtained from the PDB database.

Supplementary Material. Synthetic procedures and analytical data for intermediates reported in this article and structure determination of c-Met in complex with **23**.

ACKNOWLEDGEMENT

We thank the National Natural Science Foundation of China (81273365, 81573271, 81422047, 81321092, and 81473243), National Science & Technology Major Project ''Key New Drug Creation and Manufacturing Program'' (2014ZX09304002-008-001 and 2012ZX09301001-007), the Shanghai Science and Technology Commission (1315431901300) for their financial support. SA-SIBS Scholarship Program is also gratefully acknowledged.

REFERENCES

[1] E. Gherardi, W. Birchmeier, C. Birchmeier, G. Vande Woude, Targeting MET in cancer:

rationale and progress, Nat. Rev. Cancer 12 (2012) 89–103.

[2] L. Goyal, M.D. Muzumdar, A.X. Zhu, Targeting the HGF/c-MET pathway in hepatocellular carcinoma, Clin. Cancer. Res. 19 (2013) 2310–2318.

[3] S. Giordano, C. Ponzetto, M.F. Di Renzo, C.S. Cooper, P.M. Comoglio, Tyrosine kinase receptor indistinguishable from the c-met protein, Nature 339 (1989) 155–156.

[4] P.M. Comoglio, S. Giordano, L. Trusolino, Drug development of MET inhibitors: targeting oncogene addiction and expedience, Nat. Rev. Drug Discov. 7 (2008) 504–516.

[5] L. Trusolino, A. Bertotti, P.M. Comoglio, MET signalling: principles and functions in development, organ regeneration and cancer, Nat. Rev. Mol. Cell Biol. 11 (2010) 834–848.

[6] S. Rong, S. Segal, M. Anver, J.H. Resau, G.V. Woude, Invasiveness and metastasis of NIH 3T3 cells induced by Met-hepatocyte growth factor/scatter factor autocrine stimulation, Proc. Natl. Acad. Sci. USA 91 (1994) 4731–4735.

[7] S. Bellusci, G. Moens, G. Gaudino, P. Comoglio, T. Nakamura, J.P. Thiery, J. Jouanneau, Creation of an hepatocyte growth factor/scatter factor autocrine loop in carcinoma cells induces invasive properties associated with increased tumorigenicity, Oncogene 9 (1994) 1091–1099.

[8] M. Jeffers, S. Rong, M. Anver, W.G. Vande, Autocrine hepatocyte growth factor/scatter factor-Met signaling induces transformation and the invasive/metastastic phenotype in C127 cells, Oncogene 13 (1996) 853–856.

[9] H. Takayama, W.J. LaRochelle, R. Sharp, T. Otsuka, P. Kriebel, M. Anver, S.A. Aaronson, G. Merlino, Diverse tumorigenesis associated with aberrant development in mice overexpressing hepatocyte growth factor/scatter factor, Proc. Natl. Acad. Sci. USA 94 (1997) 701–706.

[10] T. Otsuka, H. Takayama, R. Sharp, G. Celli, W.J. LaRochelle, D.P. Bottaro, N. Ellmore, W. Vieira, J.W. Owens, M. Anver, c-Met autocrine activation induces development of malignant melanoma and acquisition of the metastatic phenotype, Cancer Res. 58 (1998) 5157–5167.

[11] J.A. Aguirre Ghiso, D.F. Alonso, E.F. Farías, D.E. Gomez, E. Bal de Kier Joffè, Deregulation of the signaling pathways controlling urokinase production, Eur. J. Biochem. 263 (1999) 295–304.

[12] C. Parr, G. Watkins, R.E. Mansel, W.G. Jiang, The hepatocyte growth factor regulatory factors in human breast cancer, Clin. Cancer. Res. 10 (2004) 202–211.

[13] R. Straussman, T. Morikawa, K. Shee, M. Barzily-Rokni, Z.R. Qian, J. Du, A. Davis, M.M. Mongare, J. Gould, D.T. Frederick, Tumour micro-environment elicits innate resistance to RAF inhibitors through HGF secretion, Nature 487 (2012) 500−504.

[14] J. Bean, C. Brennan, J.Y. Shih, G. Riely, A. Viale, L. Wang, D. Chitale, N. Motoi, J. Szoke, S. Broderick, MET amplification occurs with or without T790M mutations in EGFR mutant lung tumors with acquired resistance to gefitinib or erlotinib, Proc. Natl. Acad. Sci. USA 104 (2007) 20932–20937.

[15] J. Cui, Inhibitors targeting hepatocyte growth factor receptor and vascular endothelial growth factor receptor tyrosine kinases, Expert Opin. Ther. Pat. 16 (2006) 713–718.

[16] O. Abidoye, N. Murukurthy, R. Salgia, Review of clinic trials: agents targeting c-Met, Rev. Recent Clin. Trials 2 (2007) 143–147.

[17] J.J. Cui, Inhibitors targeting hepatocyte growth factor receptor and their potential therapeutic applications, Expert Opin. Ther. Pat. 17 (2007) 1035–1045.

[18] X. Liu, W. Yao, R.C. Newton, P.A. Scherle, Targeting the c-MET signaling pathway for

cancer therapy, Expert Opin. Investig. Drugs 17 (2008) 997–1011.

[19] J.P. Eder, G.F. Vande Woude, S.A. Boerner, P.M. LoRusso, Novel therapeutic inhibitors of the c-Met signaling pathway in cancer, Clin. Cancer. Res. 15 (2009) 2207–2214.

[20] I. Dussault, S.F. Bellon, From concept to reality: the long road to c-Met and RON receptor tyrosine kinase inhibitors for the treatment of cancer, Anticancer Agents Med. Chem. 9 (2009) 221–229.

[21] A. Giubellino, W.M. Linehan, D.P. Bottaro, Targeting the Met signaling pathway in renal cancer, Expert Rev. Anticancer Ther. 9 (2009) 785–793.

[22] X. Liu, R.C. Newton, P.A. Scherle, Developing c-MET pathway inhibitors for cancer therapy: progress and challenges, Trends Mol. Med. 16 (2010) 37–45.

[23] J. Porter, Small molecule c-Met kinase inhibitors: a review of recent patents, Expert Opin. Ther. Pat. 20 (2010) 159–177.

[24] T.L. Underiner, T. Herbertz, S.J. Miknyoczki, Discovery of small molecule c-Met inhibitors: Evolution and profiles of clinical candidates, Anticancer Agents Med. Chem. 10 (2010) 7–27.

[25] E. Ghiso, S. Giordano, Targeting MET: why, where and how?, Curr. Opin. Pharmacol. 13 (2013) 511–518.

[26] J. Zhang, P.L. Yang, N.S. Gray, Targeting cancer with small molecule kinase inhibitors, Nat. Rev. Cancer 9 (2009) 28–39.

[27] G.M. Schroeder, Y. An, Z.W. Cai, X.T. Chen, C. Clark, L.A. Cornelius, J. Dai, J. Gullo-Brown, A. Gupta, B. Henley, J.T. Hunt, R. Jeyaseelan, A. Kamath, K. Kim, J. Lippy, L.J. Lombardo, V. Manne, S. Oppenheimer, J.S. Sack, R.J. Schmidt, G. Shen, K. Stefanski, J.S. Tokarski, G.L. Trainor, B.S. Wautlet, D. Wei, D.K. Williams, Y. Zhang, Y. Zhang, J. Fargnoli, R.M. Borzilleri, Discovery of N-(4-(2-amino-3-chloropyridin-4-yloxy)-3-fluorophenyl)-4-ethoxy-1-(4-fluorophenyl)-2-oxo -1,2-dihydropyridine-3-carboxamide (BMS-777607), a selective and orally efficacious inhibitor of the Met kinase superfamily, J. Med. Chem. 52 (2009) 1251–1254.

[28] F.M. Yakes, J. Chen, J. Tan, K. Yamaguchi, Y. Shi, P. Yu, F. Qian, F. Chu, F. Bentzien, B. Cancilla, J. Orf, A. You, A.D. Laird, S. Engst, L. Lee, J. Lesch, Y.C. Chou, A.H. Joly, Cabozantinib (XL184), a novel MET and VEGFR2 inhibitor, simultaneously suppresses metastasis, angiogenesis, and tumor growth, Mol. Cancer Ther. 10 (2011) 2298–2308.

[29] R. Kurzrock, S.I. Sherman, D.W. Ball, A.A. Forastiere, R.B. Cohen, R. Mehra, D.G. Pfister, E.E. Cohen, L. Janisch, F. Nauling, D.S. Hong, C.S. Ng, L. Ye, R.F. Gagel, J. Frye, T. Muller, M.J. Ratain, R. Salgia, Activity of XL184 (cabozantinib), an oral tyrosine kinase inhibitor, in patients with medullary thyroid cancer, J. Clin. Oncol. 29 (2011) 2660–2666.

[30] J.J. Cui, M. Tran-Dube, H. Shen, M. Nambu, P.P. Kung, M. Pairish, L. Jia, J. Meng, L. Funk, I. Botrous, M. McTigue, N. Grodsky, K. Ryan, E. Padrique, G. Alton, S. Timofeevski, S. Yamazaki, Q. Li, H. Zou, J. Christensen, B. Mroczkowski, S. Bender, R.S. Kania, M.P. Edwards, Structure based drug design of crizotinib (PF-02341066), a potent and selective dual inhibitor of mesenchymal-epithelial transition factor (c-MET) kinase and anaplastic lymphoma kinase (ALK), J. Med. Chem. 54 (2011) 6342–6363.

[31] B.K. Albrecht, J.-C. Harmange, D. Bauer, L. Berry, C. Bode, A.A. Boezio, A. Chen, D. Choquette, I. Dussault, C. Fridrich, Discovery and optimization of triazolopyridazines as potent and selective inhibitors of the c-Met Kinase, J. Med. Chem. 51 (2008) 2879–2882.

[32] M.P. Lolkema, H.H. Bohets, H.T. Arkenau, A. Lampo, E. Barale, M.J. de Jonge, L. van

Doorn, P. Hellemans, J.S. de Bono, F.A. Eskens, The c-Met tyrosine kinase inhibitor JNJ-38877605 causes renal toxicity through species-specific insoluble metabolite formation, Clin. Cancer. Res. 21 (2015) 2297–2304.

[33] A.A. Boezio, L. Berry, B.K. Albrecht, D. Bauer, S.F. Bellon, C. Bode, A. Chen, D. Choquette, I. Dussault, M. Fang, S. Hirai, P. Kaplan-Lefko, J.F. Larrow, M.H. Lin, J. Lohman, M.H. Potashman, Y. Qu, K. Rex, M. Santostefano, K. Shah, R. Shimanovich, S.K. Springer, Y. Teffera, Y. Yang, Y. Zhang, J.C. Harmange, Discovery and optimization of potent and selective triazolopyridazine series of c-Met inhibitors, Bioorg. Med. Chem. Lett. 19 (2009) 6307–6312.

[34] X. Liu, Q. Wang, G. Yang, C. Marando, H.K. Koblish, L.M. Hall, J.S. Fridman, E. Behshad, R. Wynn, Y. Li, J. Boer, S. Diamond, C. He, M. Xu, J. Zhuo, W. Yao, R.C. Newton, P.A. Scherle, A novel kinase inhibitor, INCB28060, blocks c-MET-dependent signaling, neoplastic activities, and cross-talk with EGFR and HER-3, Clin. Cancer. Res. 17 (2011) 7127–7138.

[35] F. Chen, Y. Wang, J. Ai, Z. Zhan, Y. Lv, Z. Liang, C. Luo, D. Mei, M. Geng, W. Duan, O-linked triazolotriazines: potent and selective c-Met inhibitors, ChemMedChem 7 (2012) 1276–1285.

[36] E.A. Peterson, Y. Teffera, B.K. Albrecht, D. Bauer, S.F. Bellon, A. Boezio, C. Boezio, M.A. Broome, D. Choquette, K.W. Copeland, I. Dussault, R. Lewis, M.H. Lin, J. Lohman, J. Liu, M. Potashman, K. Rex, R. Shimanovich, D.A. Whittington, K.R. Vaida, J.C. Harmange, Discovery of potent and selective 8-fluorotriazolopyridine c-Met inhibitors, J. Med. Chem. 58 (2015) 2417–2430.

[37] C. Li, J. Ai, D. Zhang, X. Peng, X. Chen, Z. Gao, Y. Su, W. Zhu, Y. Ji, X. Chen, M. Geng, H. Liu, Design, synthesis, and biological evaluation of novel imidazo[1,2-a]pyridine derivatives as potent c-Met inhibitors, ACS Med. Chem. Lett. 6 (2015) 507–512.

[38] C. Birchmeier, W. Birchmeier, E. Gherardi, G.F.V. Woude, Met, metastasis, motility and more, Nat. Rev. Mol. Cell Biol. 4 (2003) 915–925.

[39] G.M. Stella, S. Benvenuti, P.M. Comoglio, Targeting the MET oncogene in cancer and metastases, Expert Opin. Investig. Drugs 19 (2010) 1381–1394.

[40] Y.W. Zhang, Y. Su, O.V. Volpert, G.F.V. Woude, Hepatocyte growth factor/scatter factor mediates angiogenesis through positive VEGF and negative thrombospondin 1 regulation, Proc. Natl. Acad. Sci. USA 100 (2003) 12718–12723.

[41] M. Stoker, E. Gherardi, M. Perryman, J. Gray, Scatter factor is a fibroblast-derived modulator of epithelial cell mobility, Nature 327 (1987) 239–242.

[42] Y.W. Zhang, G.F. Vande Woude, HGF/SF-met signaling in the control of branching morphogenesis and invasion, J. Cell. Biochem. 88 (2003) 408–417.

[43] C. Boccaccio, P.M. Comoglio, Invasive growth: a MET-driven genetic programme for cancer and stem cells, Nat. Rev. Cancer 6 (2006) 637–645.

[44] L. Trusolino, P.M. Comoglio, Scatter-factor and semaphorin receptors: cell signalling for invasive growth, Nat. Rev. Cancer 2 (2002) 289–300.

Captions

Figure 1. The representative selective c-Met inhibitors.

Figure 2. Strategies to eliminate the OCH_2-related metabolic deficiency.

Figure 3. Co-crystal structure of **23** in complex with the kinase domain of c-Met. The pdb code of the structure is 5EOB. (A) Compound **23** bound at the ATP-binding site of c-Met with a "U" shape. (B) The interactions of **23** with the surrounding residues, including two H-bonds between the compound and the backbone amide of Met1160 and Asp1222 at the hinge region and the DFG motif, respectively.

Figure 4. Compound **23** suppressed the phosphorylation of c-Met and its downstream signaling in various cells (EBC-1 Cells (A), MKN45 cells (B), BaF3/TPR-Met cells (C), and U87MG cells (D). Cells were treated with indicated concentrations of **23** for 1 h and analyzed by immunoblot.

Figure 5. Compound **23** specifically inhibited c-Met-dependent cancer cell proliferation. The anti-proliferation activity of **23** against a panel of tumor cell lines originating from different tissue types was determined by a sulforhodamine B (SRB) or an MTT assay. The IC_{50} values were plotted as the mean±SD (nM) from three separate experiments or estimated values from two separate experiments.

Figure 6. Compound **23** prevented HGF-induced migration, invasion, scattering, and invasive growth phenotypes. Compound **23** impaired migratory (A) and invasive (B) ability of NCI-H441 cells induced by 100 ng/mL of HGF (Scale bar, 100 μm); MDCK cell scattering induced by HGF was inhibited by **23** (C) (Scale bar, 10 μm); Compound **23** prevented HGF-induced branching morphogenesis (D). MDCK cells were cultured in collagen gel with 100 ng/mL of HGF, and tubule-like structure was photographed after 5-day treatment (Scale bar, 10 μm). Representative pictures presented in A−D were taken from three independent experiments.

Figure 7. Compound **23** potently inhibited c-Met-dependent tumor growth in vivo. Inhibitory activity of **23** on the tumor growth in MKN45 (A) and EBC-1 (B) xenografts. The tumor-bearing mice were administrated (po) **23** twice daily for 3 weeks. Mean relative tumor volume ± SE was shown (n = 6 in treated group, n = 12 in vehicle group). **P<0.01, ***P<0.001 vs vehicle group, determined using Student's t test.

Table 1. c-Met Enzymatic and Cellular Activities of the CH_2-Linked Triazolotriazines.

Table 2. c-Met Enzymatic and Cellular Activities of the CF_2-Linked Triazolotriazines.

Table 3. Pharmacokinetic Profiles of **23**, **25**, **26**, and **27** in Rats.

Table 4. Antitumor Efficacy of Compounds **23**, **26**, and **27** in the EBC-1 Xenograft Model.

Table 5. Kinase Selectivity Profile of **23**.

Table 6. Anti-proliferative activity of **23** on c-Met-addicted cell lines.

Scheme 1. Synthesis of Compounds **3**−**27**. Reagents and conditions: (a) 2-(quinolin-6-yl)acetic acid for **28**−**42**, 2-(1H-indol-3-yl)acetic acid for **43**−**45**, 2,2-difluoro-2-(quinolin-6-yl)acetic acid for **46**−**51**, HOBT, EDCI, DIPEA, DMF; (b) HOAc, 100 ^{o}C; (c) CF_3COOH, DCM.

Scheme 2. Optimization of Reaction Conditions for the Preparation of **23**.

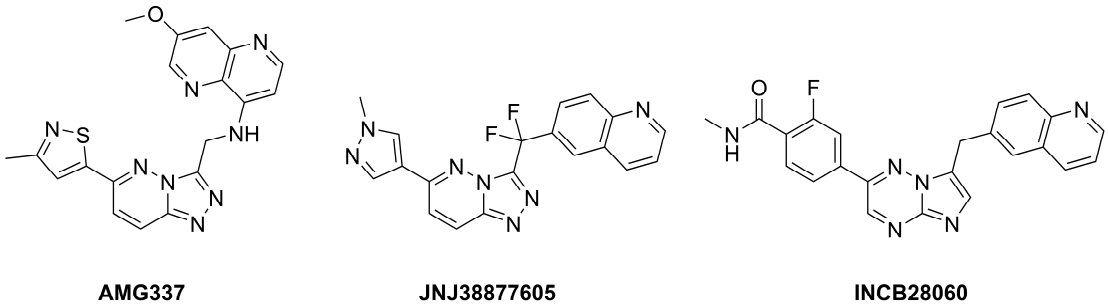

Figure 1. The representative selective c-Met inhibitors.

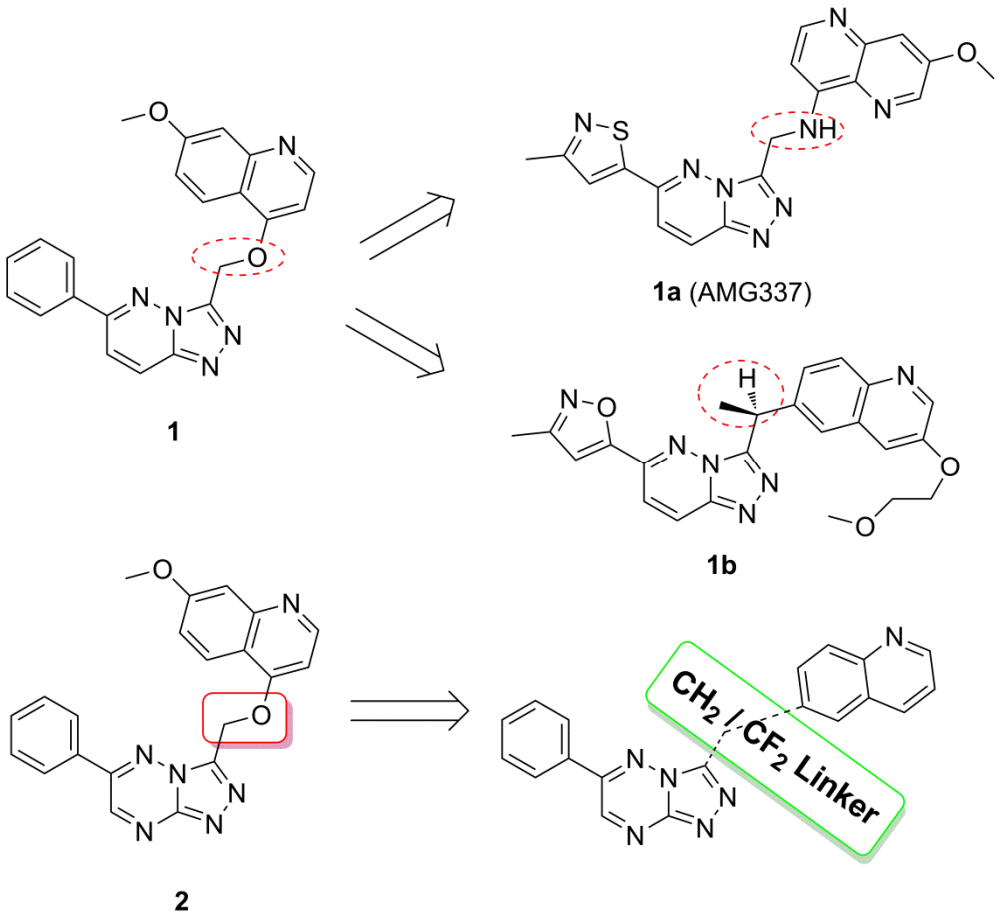

Figure 2. Strategies to eliminate the OCH_2-related metabolic deficiency.

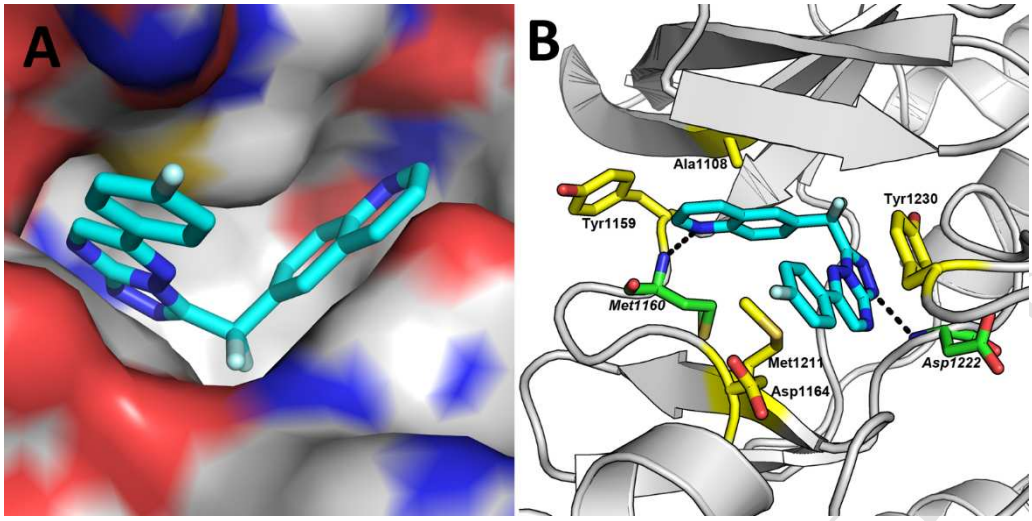

Figure 3. Co-crystal structure of **23** in complex with the kinase domain of c-Met. The pdb code of the structure is 5EOB. (A) Compound **23** bound at the ATP-binding site of c-Met with a "U" shape. (B) The interactions of **23** with the surrounding residues, including two H-bonds between the compound and the backbone amide of Met1160 and Asp1222 at the hinge region and the DFG motif, respectively.

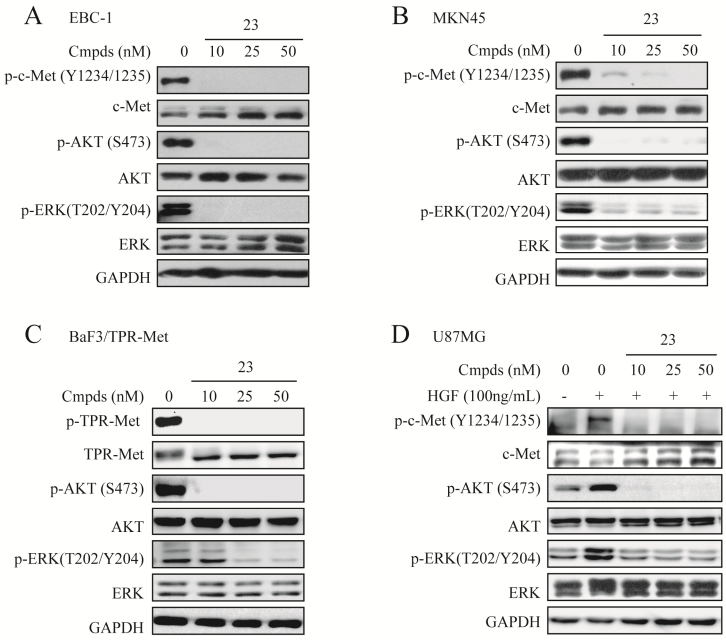

Figure 4. Compound **23** suppressed the phosphorylation of c-Met and its downstream signaling in various cells (EBC-1 Cells (A), MKN45 cells (B), BaF3/TPR-Met cells (C), and U87MG cells (D). Cells were treated with indicated concentrations of **23** for 1 h and analyzed by immunoblot.

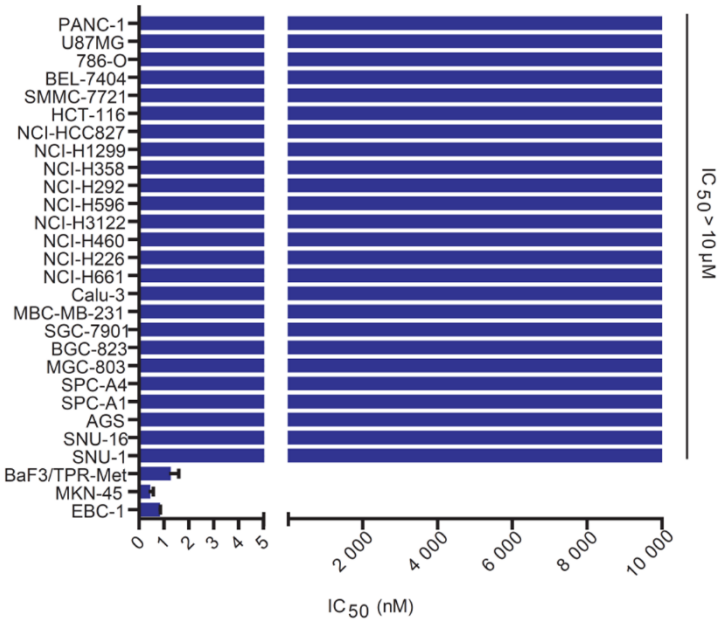

Figure 5. Compound **23** specifically inhibited c-Met-dependent cancer cell proliferation. The anti-proliferation activity of **23** against a panel of tumor cell lines originating from different tissue types was determined by a sulforhodamine B (SRB) or an MTT assay. The IC_{50} values were plotted as the mean±SD (nM) from three separate experiments or estimated values from two separate experiments.

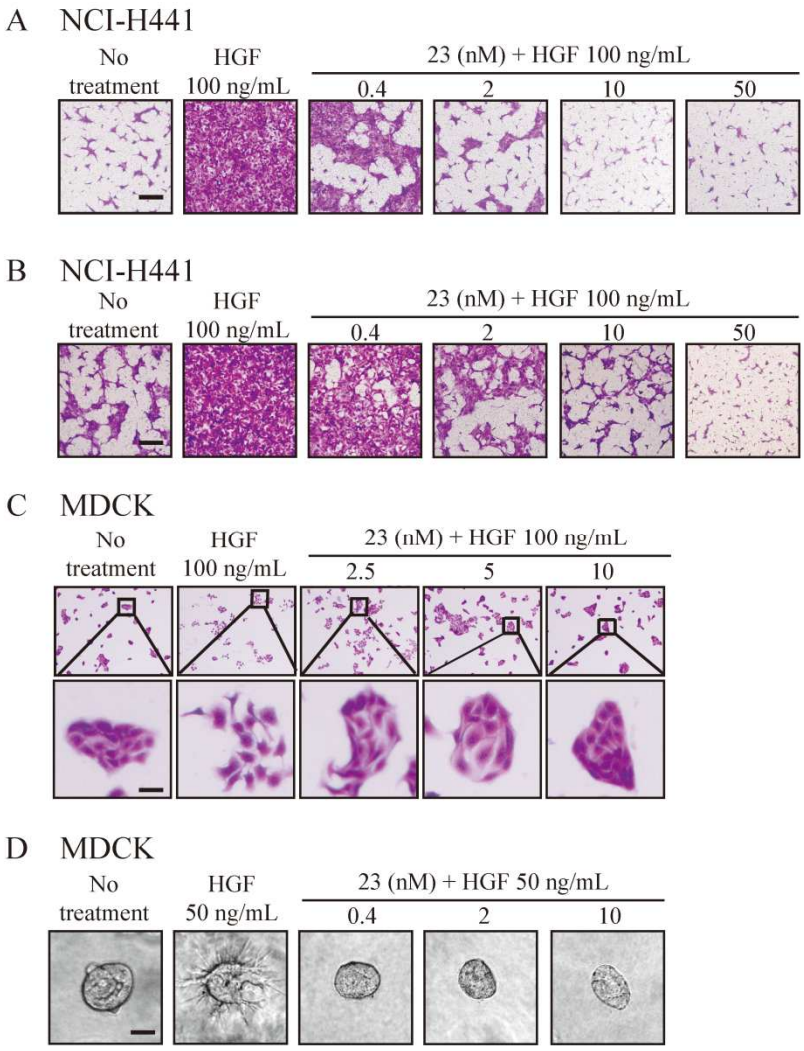

Figure 6. Compound **23** prevented HGF-induced migration, invasion, scattering, and invasive growth phenotypes. Compound **23** impaired migratory (A) and invasive (B) ability of NCI-H441 cells induced by 100 ng/mL of HGF (Scale bar, 100 μm); MDCK cell scattering induced by HGF was inhibited by **23** (C) (Scale bar, 10 μm); Compound **23** prevented HGF-induced branching morphogenesis (D). MDCK cells were cultured in collagen gel with 100 ng/mL of HGF, and tubule-like structure was photographed after 5-day treatment (Scale bar, 10 μm). Representative pictures presented in A−D were taken from three independent experiments.

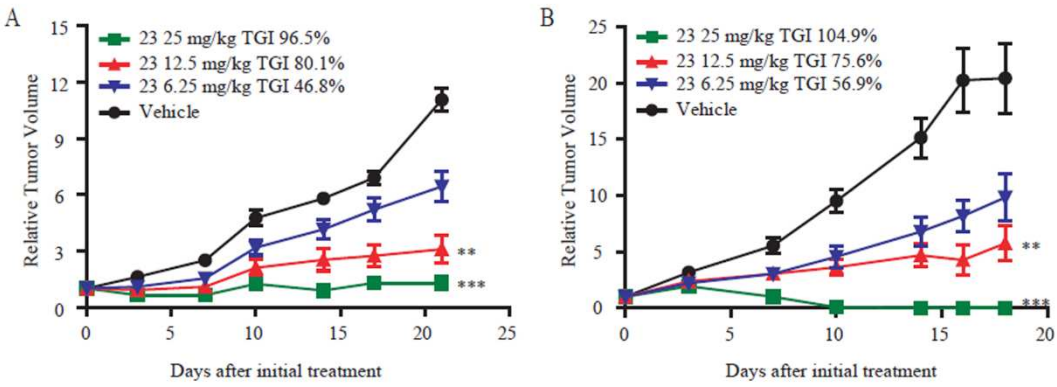

Figure 7. Compound **23** potently inhibited c-Met-dependent tumor growth *in vivo*. Inhibitory activity of **23** on the tumor growth in MKN45 (A) and EBC-1 (B) xenografts. The tumor-bearing mice were administrated (*po*) **23** twice daily for 3 weeks. Mean relative tumor volume ± SE was shown (n = 6 in treated group, n = 12 in vehicle group). ***P<0.01*, ****P<0.001* vs vehicle group, determined using Student's t test.

Table 1. c-Met Enzymatic and Cellular Activities of the CH_2-Linked Triazolotriazines[a]

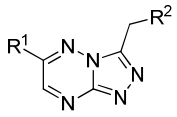

Compd.	R^1	R^2	c-Met IC_{50} (nM)	NIH3T3/TPR-Met Proliferation Inhibition (%)	
				10 μM	1 μM
2	-	-	0.19±0.02	--[b]	--[b]
3		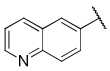	0.49±0.13	80.9	58.4
4	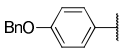	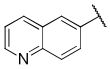	6.90±0.50	88.0	53.8
5	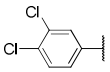	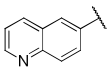	1.20±0.20	83.5	82.2
6	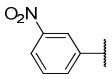	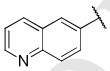	2.00±0.40	88.3	76.6
7	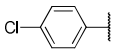	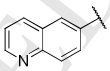	2.50±0.50	80.6	69.2
8	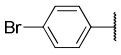	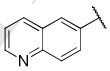	4.20±0.60	83.6	75.8
9	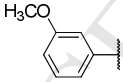	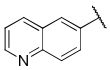	0.59±0.02	81.0	69.8
10	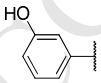	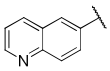	0.42±0.14	69.9	36.1
11	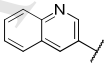	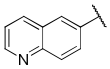	2.30±0.70	78.0	63.1
12		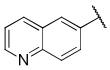	2.30±0.10	89.3	85.9
13	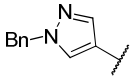	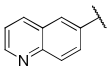	3.20±0.50	89.5	68.3

14	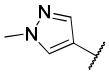	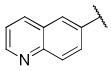	0.46±0.11	77.8	76.9
15	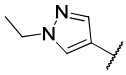	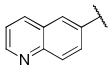	4.10±0.90	97.1	85.5
16	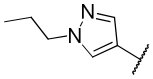	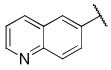	1.20±0.10	88.4	88.1
17	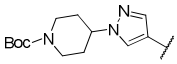	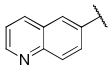	5.30±0.40	86.6	68.9
18	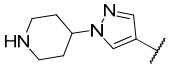	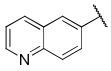	10.50±0.40	77.0	14.9
19	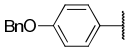		413.20±10.20	58.0	26.9
20	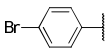		129.20±5.40	17.3	9.9
21			126.60±2.50	10.2	8.2
JNJ38877605	-	-	0.95±0.12	72.2	70.8

[a]The IC_{50} values are shown as the mean ± SD (nM) and the inhibitory rates were estimated from two separate experiments.

[b]IC_{50} value is 79.5 nM.

Table 2. c-Met Enzymatic and Cellular Activities of the CF_2-Linked Triazolotriazines[a]

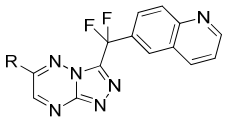

Compd.	R	c-Met IC_{50} (nM)	EBC-1 IC_{50} (nM)
22		2.80±0.10	ND[b]
23		0.24±0.04	0.85±0.01
24		1.40±0.50	ND[b]
25		0.50±0.16	0.43±0.13
26		0.50±0.10	2.30±0.11
27	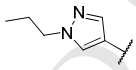	0.90±0.10	0.67±0.23
JNJ38877605	-	0.95±0.12	5.50±0.14

[a]The IC_{50}s are shown as the mean ± SD (nM). [b]Not determined.

Table 3. Pharmacokinetic Profiles of **23**, **25**, **26**, and **27** in Rats[a]

Compd.	CL[b] (L/h/kg)	V_{ss}[b] (L/kg)	$T_{1/2}$[b] (h)	C_{max}[c] (ng/mL)	T_{max}[c] (h)	$AUC_{0-\infty}$[c] (ng·hr/mL)	F^c (%)
23	2.83	4.89	1.23	869	1.00	2377	48.3
25[d]	1.34	0.81	1.14	209	2.50	780	9.4
26	2.37	5.14	1.53	961	0.42	2042	48.0
27	1.84	3.20	1.21	1614	0.50	3387	61.6

[a]Experiments were carried out in male Sprague Dawley rats (n=3); dose: *iv*, 2 mg/kg (1% (v/v) DMA, 9% (v/v) Cremophor, 90% (v/v) saline); *po*, 10 mg/kg (0.5% (w/v) CMC-Na); [b]data obtained from *iv* experiments; [c]data obtained from *po* experiments; [d]dose: *iv*, 10 mg/kg (10% (v/v) DMSO, 10% (v/v) Tween 80, 80% (v/v) (40% (w/v) PEG40); *po*, 10 mg/kg (10% (v/v) DMSO, 5% (v/v) Tween 80, 85% (v/v) saline).

Table 4. Antitumor Efficacy of Compounds **23**, **26**, and **27** in the EBC-1 Xenograft Model[a]

Compd.	Dose (mg/kg)	TGI (%)
vehicle	/	/
23	25	97.1 (2)
	12.5	76.1
26	25	65.8
	12.5	50.1
27	25	96.6 (2)
	12.5	75.9

[a]*po* administration, bid/21, "()" is the number of the mice with complete tumor regression

Table 5. Kinase Selectivity Profile of **23**[a]

kinase	IC_{50} (nM)	kinase	IC_{50} (nM)
c-Met	0.24±0.04	ErbB2	31.5%@1000nM
RON	33.9%@1000nM	ErbB4	26.8%@1000nM
AXL	36.0%@1000nM	FGFR1	12.8%@1000nM
Tyro3	10.1%@1000nM	RET	29.9%@1000nM
Mer	13.5%@1000nM	KDR	15.3%@1000nM
IGF1R	0.4%@1000nM	Flt-1	11.5%@1000nM
ALK	2.1%@1000nM	Flt-3	12.3%@1000nM
ROS1	10.6%@1000nM	c-Kit	32.1%@1000nM
PDGFR-α	31.4%@1000nM	c-Src	13.7%@1000nM
PDGFR-β	19.6%@1000nM	ABL	14.9%@1000nM
EGFR	33.2%@1000nM	EPH-A2	6.1%@1000nM
EGFR/T790M-L858R	28.9%@1000nM	EPH-B2	8.5%@1000nM

[a]The ability of **23** to inhibit the enzymatic activities of a panel of recombinant tyrosine kinases was evaluated by ELISA assays, representing IC_{50}s as mean ± SD or estimated values from two separate experiments.

Table 6. Anti-proliferative activity of **23** on c-Met-addicted cell lines[a]

Compd.	IC_{50} (nM)		
	EBC-1	MKN45	BaF3/TPR-Met
23	0.85±0.01	0.46±0.12	1.28±0.32
JNJ38877605	5.50±0.14	9.50±2.00	8.60±1.40

[a]IC_{50} values were shown as mean ± SD from three separate experiments.

Scheme 1. Synthesis of Compounds **3**−**27**[a]

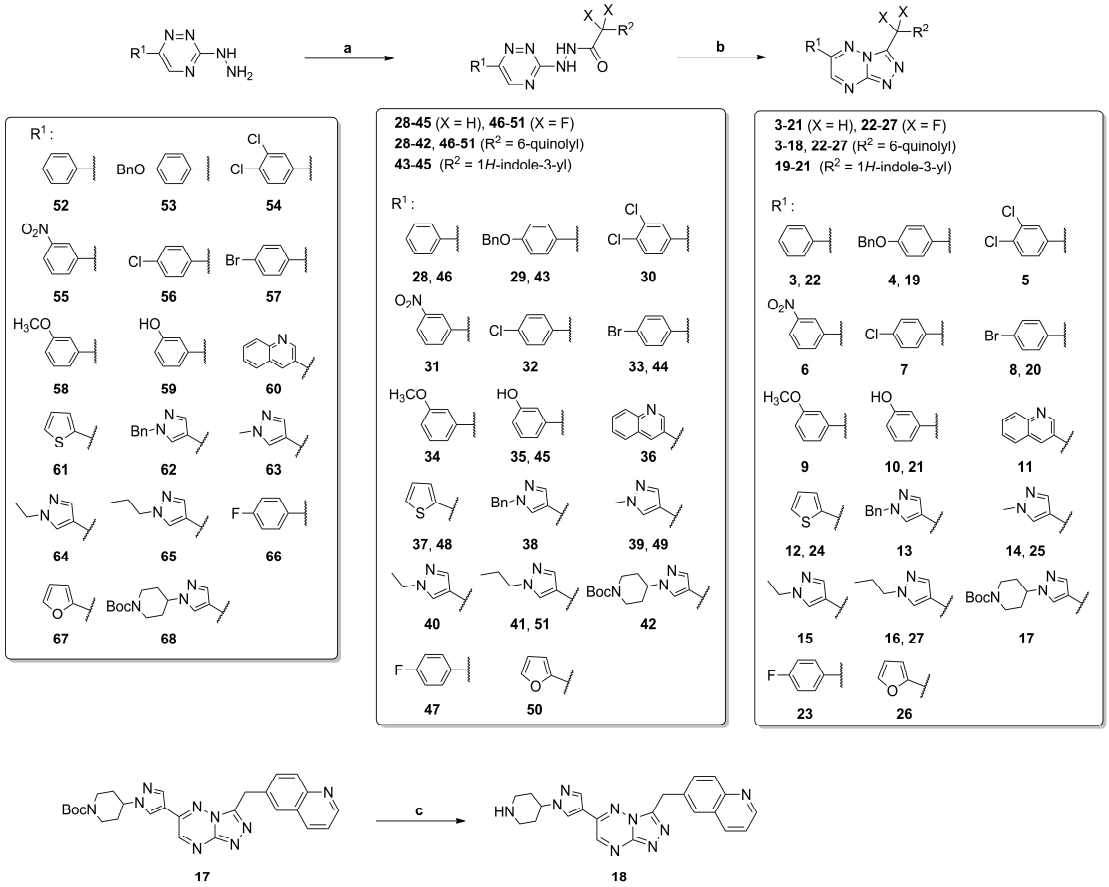

[a]Reagents and conditions: (a) 2-(quinolin-6-yl)acetic acid for **28**−**42**, 2-(1H-indol-3-yl)acetic acid for **43**−**45**, 2,2-difluoro-2-(quinolin-6-yl)acetic acid for **46**−**51**, HOBT, EDCI, DIPEA, DMF; (b) HOAc, 100 ^{o}C; (c) CF_3COOH, DCM.

Scheme 2. Optimization of Reaction Conditions for the Preparation of **23**

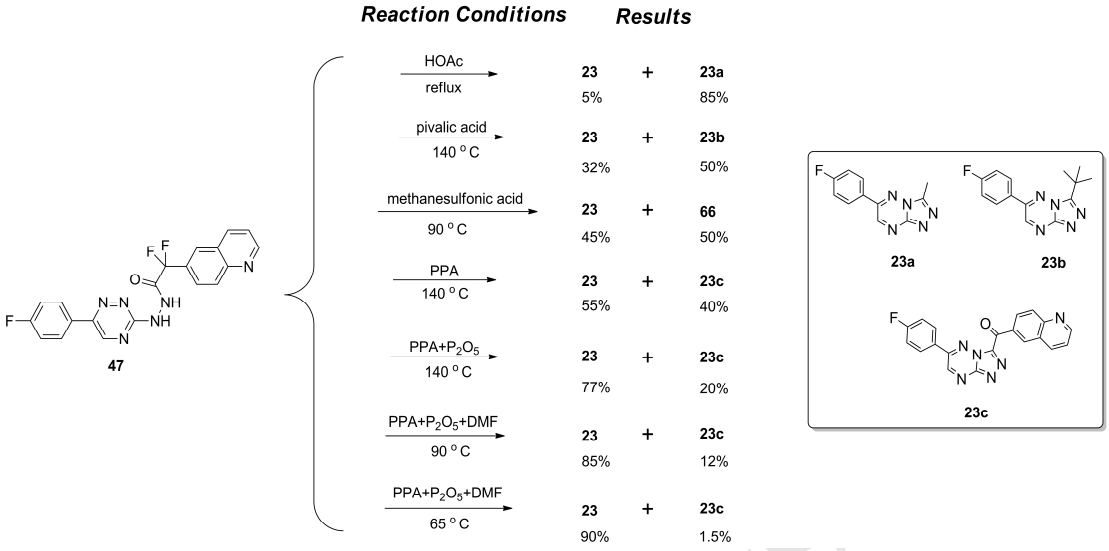

A series of CH_2- / CF_2-linked triazolotriazines as c-Met inhibitors were reported.

The compounds were assayed c-Met activities in both enzymatic and cellular level.

Based on good antitumor potency and PK profiles, **23** was selected as a drug candidate.